© 2019. Published by The Company of Biologists Ltd | Development (2019) 146, dev173286. doi:10.1242/dev.173286

RESEARCH ARTICLE

yap1b, a divergent Yap/Taz family member, cooperates with *yap1* in survival and morphogenesis via common transcriptional targets

Javier Vázquez-Marín[1], José Arturo Gutiérrez-Triana[2,4], María Almuedo-Castillo[1], Lorena Buono[1], José Luis Gómez-Skarmeta[1], Juan Luis Mateo[2,3], Joachim Wittbrodt[2] and Juan Ramón Martínez-Morales[1,*]

ABSTRACT

Yap1/Taz are well-known Hippo effectors triggering complex transcriptional programs controlling growth, survival and cancer progression. Here, we describe *yap1b*, a new Yap1/Taz family member with a unique transcriptional activation domain that cannot be phosphorylated by Src/Yes kinases. We show that *yap1b* evolved specifically in euteleosts (i.e. including medaka but not zebrafish) by duplication and adaptation of *yap1*. Using DamID-seq, we generated maps of chromatin occupancy for Yap1, Taz (Wwtr1) and Yap1b in gastrulating zebrafish and medaka embryos. Our comparative analyses uncover the genetic programs controlled by Yap family proteins during early embryogenesis, and show largely overlapping targets for Yap1 and Yap1b. CRISPR/Cas9-induced mutation of *yap1b* in medaka does not result in an overt phenotype during embryogenesis or adulthood. However, *yap1b* mutation strongly enhances the embryonic malformations observed in *yap1* mutants. Thus *yap1*$^{-/-}$; *yap1b*$^{-/-}$ double mutants display more severe body flattening, eye misshaping and increased apoptosis than *yap1*$^{-/-}$ single mutants, thus revealing overlapping gene functions. Our results indicate that, despite its divergent transactivation domain, Yap1b cooperates with Yap1 to regulate cell survival and tissue morphogenesis during early development.

KEY WORDS: Yap/Taz, Chromatin binding, Morphogenesis, Apoptosis, Transcriptional activation domain, DamID-seq

INTRODUCTION

The Yap/Taz family of transcriptional co-activators plays a key role during embryogenesis, acting as master regulators of growth, cell fate specification and survival, as well as in adult organs, where they are crucial for tissue repair and cancer progression (Piccolo et al., 2014; Varelas, 2014; Zanconato et al., 2016). The Yes-associated protein 1 (Yap1 or Yap) was the first member of the family identified on the basis of its interaction with members of the Src/Yes protein tyrosine kinase family (Sudol, 1994). A few years later, a second paralog of the family, Taz (transcriptional co-activator with PDZ-binding domain; also known as WW domain-containing transcription regulator protein 1 or Wwtr1), was identified through the interaction with 14-3-3 (Kanai et al., 2000). Yap and Taz share a very similar domains structure, including N-terminal Tead- and 14-3-3-binding domains, one or two WW domains, and a C-terminal transcriptional activation domain that ends in a short PDZ-domain recognition sequence (Fig. 1). Yap/Taz, as well as their *Drosophila* ortholog Yorkie (Huang et al., 2005), do not contain a DNA-binding domain and hence need to be associated to a transcription factor to exert their regulatory function. Pioneer work revealed the interaction between the Yap N terminus and the four members of the Tead family of transcription factors in vertebrates (Vassilev et al., 2001). Furthermore, the study determined that the C-terminal acidic domain in Yap is in fact the transcriptional activation domain for Tead proteins (Vassilev et al., 2001). This interaction was further confirmed for the corresponding orthologs in *Drosophila*: Yorkie and Scalloped (Bandura and Edgar, 2008; Zhang et al., 2008). Although Yap/Taz activity can be modulated by a number of transcription factors, including members of the AP-1, Runx, β-catenin, Tbx, p53 and Smad families (Piccolo et al., 2014), only its association to Tead has been proved to be essential for chromatin-binding and transcriptional effects (Galli et al., 2015; Li et al., 2010; Stein et al., 2015; Zanconato et al., 2015; Zhao et al., 2008).

One of the most relevant features of the Yap/Taz-Tead module is its ability to integrate upstream information from signaling pathways and structural cell properties, such as cell adhesion, density, polarity, contractility and shape, into a contextual transcriptional response. This is achieved through a number of regulatory inputs, with the Hippo pathway being the best understood of them. The core components of the Hippo pathway were identified due to the striking tissue overgrowth observed in *Drosophila* mutants (Harvey et al., 2003; Tapon et al., 2002; Wu et al., 2003). This evolutionary conserved signaling cascade is regulated by two sequential kinases, Mst1/2 and Lats1/2 (Hippo and Warts respectively in *Drosophila*), which converge in the phosphorylation of Yap/Taz and result in its sequestration and/or degradation in the cytoplasm. When the inhibitory pathway is not active, Yap/Taz are free to shuttle from the cytoplasm to the nucleus and to exert their role as transcriptional co-activators (Meng et al., 2016). Apart from the Hippo pathway, the activity of the Yap/Taz is controlled by many other factors, most notably mechanical cues. Yap/Taz translocation to the nucleus is regulated by cell geometry, being active in cells that have undergone cell spreading and inactive in round and compact cells (Dupont et al., 2011). The ability of Yap/Taz to sense mechanical tension depends on myosin contractility, actin-capping and -severing proteins, and the integrin-talin mechanosensitive clutch (Aragona et al., 2013; Dupont et al., 2011; Elosegui-Artola et al., 2016). Moreover, recent work has shown that mechanical coupling between the ECM and the nuclear envelope is responsible for Yap/Taz nuclear translocation across nuclear pores, a process that does not depend on the activity of the Hippo pathway (Elosegui-Artola et al., 2017).

A second Hippo-independent regulatory input on Yap/Taz comes from members of the Src family of tyrosine kinases (SFKs). As

[1]Centro Andaluz de Biología del Desarrollo (CSIC/UPO/JA), 41013 Seville, Spain. [2]Centre for Organismal Studies (COS), University of Heidelberg, 69120 Heidelberg, Germany. [3]Departamento de Informática, Universidad de Oviedo, Oviedo 33005, Spain. [4]Escuela de Microbiología, Facultad de la Salud, Universidad Industrial de Santander, Bucaramanga, 680002, Colombia.

*Author for correspondence (jrmarmor@upo.es)

M.A.-C., 0000-0001-6759-5879; J.L.G.-S., 0000-0001-5125-4332; J.L.M., 0000-0001-9902-6048; J.W., 0000-0001-8550-7377; J.R.M.-M., 0000-0002-4650-4293

Received 30 October 2018; Accepted 17 May 2019

Development (2019) 146, dev173286. doi:10.1242/dev.173286

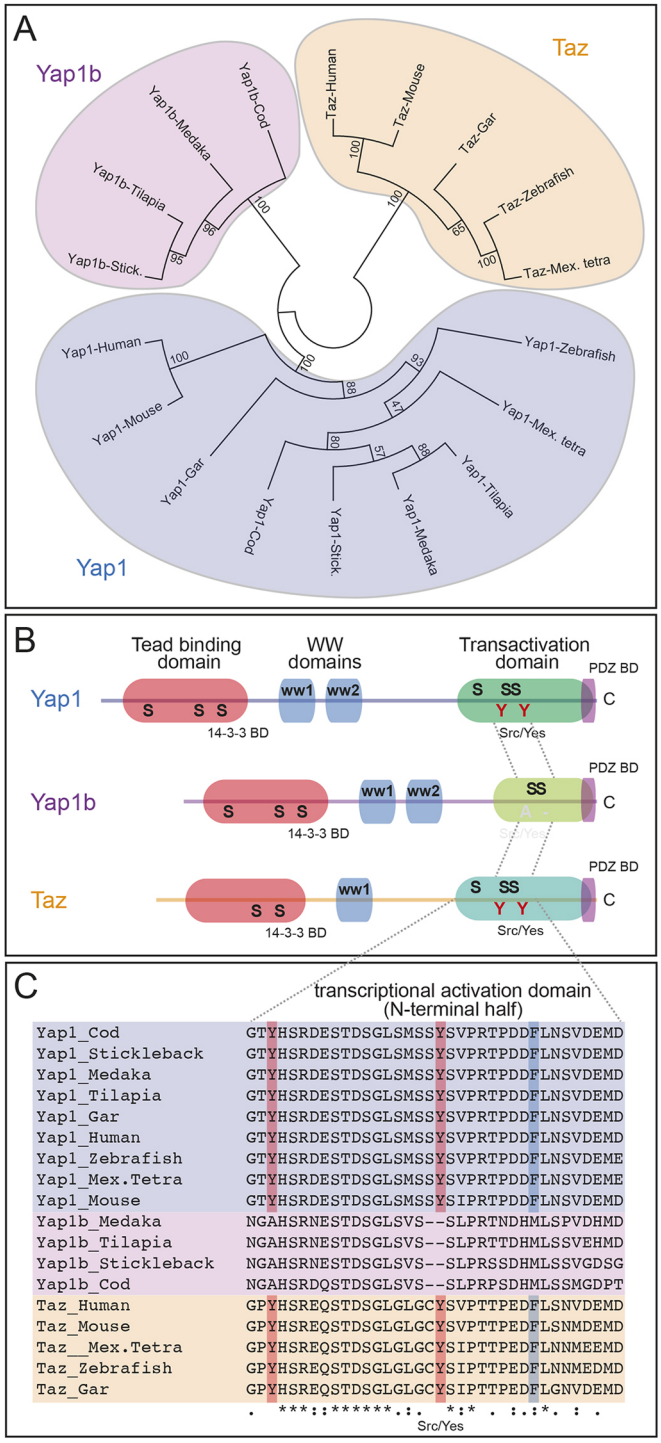

Fig. 1. Phylogenetic analysis of the Yap family in teleosts. (A) Maximum-likelihood analysis defines three Yap-related subfamilies: Yap1, Taz and Yap1b. (B) The scheme summarizes the domain architectures of Yap1, Yap1b and Taz, emphasizing the divergent sequence of the C-terminal transactivation domain in Yap1b (green). (C) Multiple sequence alignment of the N-terminal segment of the transactivation domain shows the atypical Yap1b sequence. There is elimination or substitution of conserved tyrosine (red) and phenylalanine (blue) residues (see also Fig. S3D).

already mentioned, Yap was initially identified as a Yes- and Src-interacting protein (Sudol, 1994). A number of SFKs, including c-Abl, Src and Yes, have been shown to phosphorylate Yap in a specific tyrosine residue (Y357 in humans) located at the C-terminal transcriptional activation domain (Levy et al., 2008; Rosenbluh et al., 2012; Vlahov et al., 2015; Zaidi et al., 2004). More recently, Src-mediated phosphorylation of the three conserved tyrosine residues (including Y357) of the Yap C-terminal domain has been reported in keratinocytes (Li et al., 2016). In contrast to the inhibitory role of the Hippo pathway, SFK-mediated phosphorylation of Yap results in the transcriptional activation of Yap/Tead (Calvo et al., 2013; Li et al., 2016; Tamm et al., 2011), Yap/Runx2 (Zaidi et al., 2004), Yap/p73 (Levy et al., 2008) or Yap/β-Catenin/Tbx5 complexes (Rosenbluh et al., 2012; Vlahov et al., 2015). Importantly, It has been suggested that Yap phosphorylation by Src may mediate the oncogenic activity of the kinase (Li et al., 2016), which is in agreement with the pervasive activation of Yap in cancerous cells (Zanconato et al., 2016).

Phylogenetic analysis has shown an ancient evolutionary history for the Yap-Tead module. Bona fide orthologs of Tead are already present in yeast, whereas Yap-related proteins can be traced back to basal metazoans such as Nematostella (Hilman and Gat, 2011). Despite this general conservation, significant differences have also been reported. Importantly for this work, the conserved tyrosine residues required for SFKs phosphorylation appear to be a vertebrate innovation in the C-terminal region of Yap/Taz (Elbediwy and Thompson, 2018; Hilman and Gat, 2011). The vertebrate paralogs *Yap* and *Taz* emerged after the two rounds of whole-genome duplication that occurred in the stem of the lineage (Dehal and Boore, 2005). Data from different vertebrate models indicate that *Yap* and *Taz* have partially overlapping roles during development. Individual mutations of *Yap* and *Taz* in mice result in very different phenotypes: from defects in elongation, impaired yolk sac vasculogenesis and lethality at day 8.5 in $Yap^{-/-}$ embryos, to polycystic kidneys and premature death in $Taz^{-/-}$ adults (Morin-Kensicki et al., 2006; Xin et al., 2013). However, the strong phenotype observed in both double mutant embryos (i.e. lethality prior to the morula stage) (Nishioka et al., 2009) and in tissue-specific double knockouts (Deng et al., 2017; Lee et al., 2016; Singh et al., 2016) indicate functional redundancy for *Yap* and *Taz*. The same paralogs, *yap* and *taz*, have been reported in teleosts. Similarly to mammalian genes, zebrafish paralogs seem to play redundant roles, severely impairing early development when they are inactivated simultaneously (Kimelman et al., 2017; Miesfeld et al., 2015).

Here, we analyze the distribution of Yap family proteins in teleosts and describe Yap1b as a new paralog with an atypical transcriptional activation domain. We use DamID-seq to characterize, early during development, the DNA sites targeted by Yap1 and Yap1b in the medaka genome, as well as by Yap1 and Taz in the zebrafish genome. We show that CRISPR/Cas9-induced mutation of *yap1b* in medaka neither results in apparent embryonic defects nor affects adult fish survival and fertility. However, simultaneous mutation of *yap1* and *yap1b* leads to enhanced apoptosis and deeper morphogenetic defects, indicating that both paralogs cooperate during early embryogenesis in medaka.

RESULTS

Identification of Yap1b as a new member of the Yap protein family

Medaka embryos carrying a nonsense mutation for *yap1* (i.e. a premature stop codon at the WW1 domain), named *hirame* (*hir*), display deep phenotypic malformations, including optic cup flattening, lens misalignment, delayed blastopore closure and increased cell death early during development (Porazinski et al., 2015). We confirmed these results by generating two additional *yap1* mutant alleles using CRISPR/Cas9 in medaka. The chromosomal lesions consist of 7 and 11 bp deletions in exon 2

Development (2019) 146, dev173286. doi:10.1242/dev.173286

that result in frameshift mutations and premature stop codons before the WW1 domain of the protein (Fig. S1A,B). Both alleles showed a phenotype very similar to the previously described mutation *hir*, with the exception that the blastopore closure defects observed are very mild (Fig. S1C-H). The strong phenotype displayed in *yap1* medaka mutants was much more severe compared with the milder defects observed in zebrafish upon *yap1* mutation, and rather resembled the malformations observed in double *yap1*/*taz* mutants in zebrafish (Agarwala et al., 2015; Kimelman et al., 2017; Miesfeld et al., 2015).

To investigate whether the phenotypic discrepancy between medaka and zebrafish mutants could be due to a different contribution from paralogs, we carried out a phylogenetic analysis of the Yap protein family in teleosts. A maximum likelihood phylogenetic tree was constructed using multiple sequence alignment of proteins from seven representative teleost species. Human and mouse sequences were also included as an external reference. In spite of previous reports describing two paralogs, Yap and Taz (Wwtr1), in all vertebrates, our phylogenetic analysis unambiguously identified three distinct groups of proteins: a first group clustering all proteins annotated as Yap1; a second including Taz proteins; and a third here termed Yap1b, as it showed higher sequence homology to Yap1 than to Taz (Fig. 1A). We could identify the presence of genes encoding Yap1b proteins in all species examined from the Euteleosteomorpha clade (i.e. cod, medaka, tilapia and stickleback), the largest group within teleosts (Betancur et al., 2017). This suggests the possibility of *yap1b* emerging after the teleost-specific genome duplication (Amores et al., 1998). To test this hypothesis, we examined the syntenic arrangement of the genomic region containing Yap family genes in teleosts. Conserved synteny indicates that the loci containing *yap1* and *yap1b* derived from a common ancestor after the teleost genome duplication, whereas Taz genes show an independent genome arrangement (Fig. S2). This result confirms that, in contrast to previous assumptions (Porazinski et al., 2015; Webb et al., 2011), the second paralog present in the medaka genome is not orthologous to *taz* but rather to *yap1b*.

We then examined the structure of Yap1b proteins. Multiple sequence alignments showed relatively well-conserved N-terminal Tead and WW domains for Yap1b. In particular, the Tead binding domain of the protein is more similar to that of Yap1 than to the Taz domain, showing average identities of 65.5% and 40.3%, respectively (Fig. S3). However, the transcriptional activation domain of Yap1b seems less conserved when compared with Yap1 and Taz equivalent regions (i.e. average identities 44.8% and 23.4%, respectively). Remarkably, all conserved tyrosine residues that can be phosphorylated by kinases of the Src family, and even the structurally related phenylalanine residues, are substituted by other conserved residues or eliminated in the transcriptional activation domain of Yap1b (Fig. 1B,C; Fig. S3D). These modifications are predicted to have a significant impact on the regulatory properties of the protein, as SFK-mediated phosphorylation plays a key role in the transcriptional activation of Yap/Tead complexes (Li et al., 2016).

To gain insight into the evolutionary history of Yap family proteins, particularly into the evolution of Yap1b, we scanned the genomes of four additional species that belong to key branches of the teleost phylogenetic tree (Fig. S4): Japanese eel (*Anguilla japonica*; Elopomorpha); elephantfish (*Paramormyrops kingsleyae*; Osteoglossomorpha); herring (*Clupea harengus*; Otomorpha: Cupleiformes); and northern pike (*Esox lucius*; Euteleosteomorpha: Protacanthopterygii). Multiple sequence analyses of the transcriptional activation domain N-terminal region of Yap-related proteins revealed the presence in basal teleosts (i.e. japanese eel and elephantfish) of four paralogs, likely arising by duplication of the original *Yap* and *Taz* (Fig. S4; Table S1). Based on the overall sequence conservation and on key reference residues, we could identify genes encoding both Yap1 and Yap1b in the basal teleost genomes. Nevertheless, the transcriptional activation domain of Yap1b seems less divergent in these species, and tyrosine and phenylalanine residues are partially conserved (Fig. S4A). Our analyses are consistent with the evolutionary loss of *yap1b* in the entire Otomorpha lineage, which comprises more than 8000 living species (including herring, mexican tetra and zebrafish). They are also consistent with the evolutionary divergence of Yap1b transcriptional activation domain early in the Euteleosteomorpha lineage (including pike, cod, medaka, tilapia and stickleback). Finally, although the evolutionary history of Taz paralogs seems complex and may require further investigation, it appears that both copies were lost sequentially during teleost evolution. Thus, only one copy is present in the Otomorpha group and none in Percomorpha (i.e. ≈15,000 species, one out of four vertebrate species) (Fig. S4B). In summary, our phylogenetic analyses reveal a complex evolutionary history for Yap family proteins in teleosts, and identify the emergence in Euteleosteomorpha of Yap1b, a paralog with a divergent transcriptional activation domain.

Expression analysis of *yap1* and *yap1b* during early development

To understand the role of *yap1b* during early embryogenesis in medaka, we focused our expression studies on the developmental window extending from late gastrulation (stage 15-16) to optic cup stages (stage 23-24). This developmental period corresponds to the stages when morphogenetic defects first become apparent both in $yap1^{-/-}$ medaka embryos (Porazinski et al., 2015) and $yap^{-/-}$; $taz^{-/-}$ zebrafish embryos (Kimelman et al., 2017). Previous expression studies in zebrafish reported a *yap1* broad tissue distribution, with an enriched expression at the neural plate and axial mesoderm (Kimelman et al., 2017; Thisse et al., 2001). To extend these observations to medaka embryos, we investigated *yap1* and *yap1b* expression by *in situ* hybridization and qPCR (Fig. 2). *In situ* hybridization analysis at late gastrula stages revealed that medaka *yap1* and *yap1b* display a similar expression pattern to their zebrafish ortholog *yap1*, being broadly expressed, yet enriched, at the axial mesoderm (Fig. 2A-B′). We then examined *yap1* and *yap1b* relative transcript levels at three developmental stages by qPCR: before the onset of zygotic transcription (stage 7), at late gastrula (stage 16) and at optic cup stages (stage 24). This analysis revealed that, whereas *yap1* levels are relatively constant, *yap1b* shows a high maternal contribution and is expressed at low levels once the zygotic transcription starts (Fig. 2C,D). For comparative purposes, similar quantitative analyses were performed in zebrafish for *yap1* and *taz* at equivalent developmental stages. This analysis revealed that, in contrast to *taz*, *yap1* has a strong maternal contribution (Fig. 2E,F). To achieve an accurate measurement of RNA levels, we performed a digital droplet PCR (ddPCR) study (Pinheiro et al., 2012). This approach confirmed our qPCR observations and allowed us to estimate the relative proportion of each paralog in medaka and zebrafish (Fig. 2G,H). Our data indicate that zebrafish *yap1* and *taz* are expressed at similar levels after the maternal-to-zygotic transition (MZT). In contrast, and despite being strongly contributed by the mother, medaka *yap1b* is expressed only at low levels after MZT. This observation alone could explain the strong phenotype observed upon *yap1* mutation in medaka.

Development (2019) 146, dev173286. doi:10.1242/dev.173286

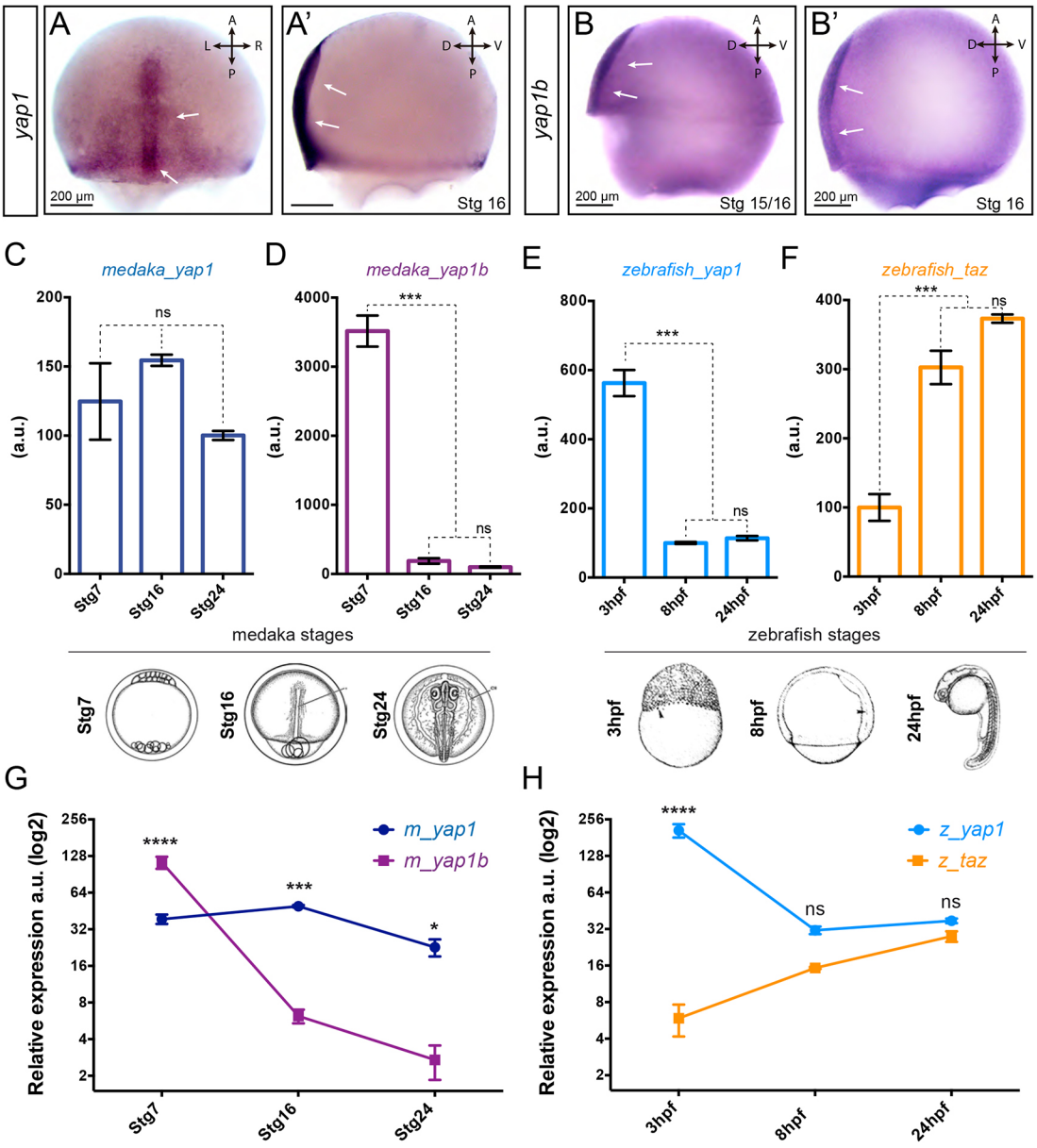

Fig. 2. Expression analysis of Yap family genes. *In situ* hybridization analysis of *yap1* (A,A′) and *yap1b* (B,B′) distribution in stage 15-16 medaka embryos. Scale bars: 200 µm. Quantification of the expression levels of Yap family genes at three equivalent developmental stages (i.e. early morula, late gastrula and optic cup stages) in medaka (C,D) and zebrafish (E,F) embryos by qPCR-RT (n=3). Relative expression level between paralogous genes was determined in medaka (G) and zebrafish (H) samples by droplet digital PCR (ddPCR) (n=2). One-way ANOVA analysis followed by Fisher's LSD test was used to evaluate statistical significance. ****P<0.0001; ***P<0.001; *P<0.05; ns, not significant.

DamID-seq profiling of chromatin-binding sites associated with Yap family proteins during early embryogenesis in teleosts

To investigate the regulatory properties of Yap family proteins in teleosts, particularly those of Yap1b, we characterized their target sites in the genome. As ChIP-grade antibodies are not available for Yap proteins in teleosts, we used DamID-seq to profile their binding. The DNA adenine methyltransferase identification (DamID) method was initially developed in *Drosophila* (van Steensel et al., 2001), and it is based on the expression of transcription factors and chromatin modifiers tethered to the bacterial DAM methylase. Although extensively used in *Drosophila* (Aughey and Southall, 2016), the technique has only recently been adapted for *in vivo* studies in vertebrates (Gutierrez-Triana et al., 2016; Tosti et al., 2018). In this work, we followed the iDamID-seq/iDEAR pipeline, first established in medaka (Gutierrez-Triana et al., 2016). We generated mycDAM-tagged constructs for medaka *DAM:yap1* and *DAM:yap1b*, and injected their corresponding mRNAs, as well as the control *DAM:GFP* mRNA, into one-cell stage medaka embryos. Proper shuttling of the fusion proteins to the nucleus was confirmed by following either DAM:GFP signal (Fig. S5A) or Myc-associated immunoreactivity (Fig. S5B). Embryos (~40 per experimental condition) were harvested at 80% epiboly (stage 16) to capture DNA occupancy throughout gastrulation. For comparative purposes, DamID-seq experiments were carried out in zebrafish, also using 80% epiboly embryos (8 hpf), injected with *DAM:yap1*, *DAM:taz* and *DAM:GFP* mRNAs at the one-cell stage. After isolation and amplification of Dam methylated regions in three independent

Development (2019) 146, dev173286. doi:10.1242/dev.173286

biological replicates (Fig. S6), samples were submitted for deep sequencing and retrieved reads were mapped on the medaka and zebrafish reference genomes. The correlation of mapped reads was high among replicas (i.e. above 70%), whereas it was very low when compared with the corresponding *DAM:GFP* controls (Fig. S7).

We used the iDEAR pipeline (Gutierrez-Triana et al., 2016) to identify differentially methylated peaks for each Yap family regulator. A representative genome browser example of peaks identified at the locus of *amotl2a*, a known Yap1 transcriptional target, is shown both for medaka and zebrafish (Fig. 3A,B); additional medaka examples for the known targets *ctgfa*, *cyr61*, *lats2*, *ccne1*, *boka* and *yap1* itself are provided in Fig. S8.

A total of 4212 and 3792 DamID peaks were identified in the medaka genome for Yap1 and Yap1b, respectively, and 7553 and 8608 in the zebrafish genome for Yap1 and Taz, respectively (Table 1, Table S5). In medaka, we found a large overlap between Yap1 and Yap1b peaks (i.e. ≈65% of the Yap1b peak was also positive for Yap1), whereas only 28.6% of the Yap1 peaks are also targeted by Taz in zebrafish (Fig. 3C, Fig. S9A,B). The overlap between the identified DamID peaks and 80% epiboly ATAC-seq marks, which are available in medaka and zebrafish (Marlétaz et al., 2018), was also calculated. Approximately 42% and 45% of the Yap1 and Yap1b peaks, respectively, overlap with open chromatin regions in medaka (Fig. 3D,E); and 49% and 25% of the Yap1 and Taz peaks, respectively, extend over ATAC regions in zebrafish. A comparative analysis of peak distribution according to the distance to their closest transcription start site (TSS) revealed an enrichment of Yap-binding sites at promoters and proximal enhancers with respect to the Dam:GFP controls (Fig. S9C-F).

We used DREME (Bailey, 2011) to identify significantly enriched motifs in the collection of peaks targeted by the different Yap family proteins (Fig. 4, Fig. S10). Among the most enriched motifs for medaka Yap1 and Yap1b, the top hits corresponded to the consensus DNA sequence of TEAD proteins: DREME E-values 5.3×10^{-143} and 5.1×10^{-98}, respectively (Fig. 4A,B). Further analyses revealed that a significantly large proportion of the Yap1 and Yap1b peaks contain the TEAD motif, particularly those regions with higher score in the iDEAR pipeline (Fig. 4C). Besides TEAD factors, a number of known motifs showed less significant enrichment in peaks targeted only by Yap1 (e.g. RREB1, TBX and ZNF143), by Yap1b (e.g. GATA2, OTX2 and TP73) or by both (e.g. POU and SOX) (Fig. 4A,B). In contrast to medaka paralogs, the search for

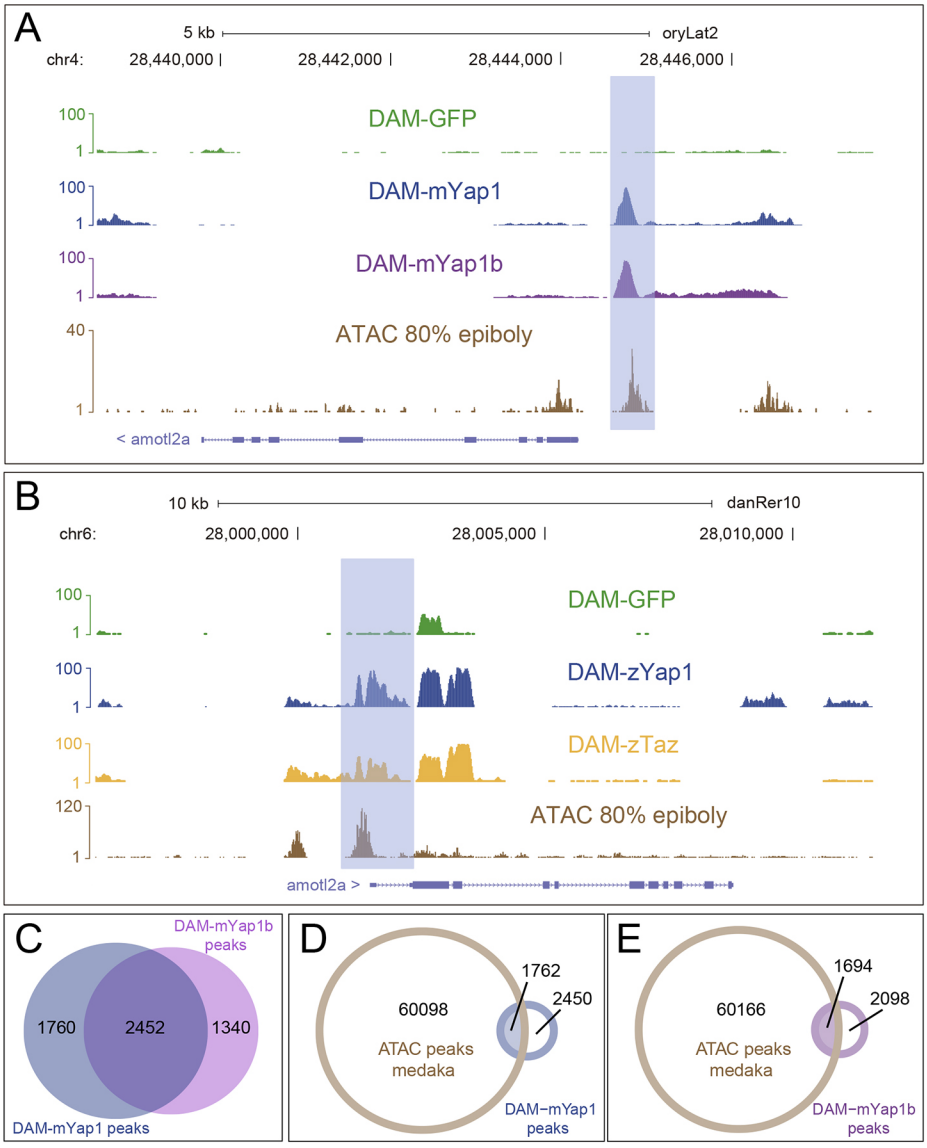

Fig. 3. DamID-seq profiling of Yap family proteins. (A,B) DamID-seq tracks from medaka and zebrafish samples are shown in the locus of *amotl2a,* a known target gene for Yap. Dam-yap1, Dam-yap1b and Dam-GFP peaks generated from 80% epiboly medaka embryos (A), as well as Dam-yap1, Dam-Taz and Dam-GFP peaks from 80% epiboly zebrafish embryos (B) are shown in relation to available ATAC-seq marks in each species. There are differentially methylated peaks (shadow boxes), in the vicinity of the *amotl2a* promoter. (C) Venn diagram shows a large overlap between Dam-yap1 and Dam-yap1b peaks. (D,E) The overlap between ATAC-seq marks and both Dam-yap1 (D) and Dam-yap1b (E) peaks is also represented.

Development (2019) 146, dev173286. doi:10.1242/dev.173286

Table 1. Number of peaks identified by iDEAR and number of genes associated with each peak for the different Yap family members

	Number of peaks identified by iDEAR	Number genes associated with peaks
Medaka Yap1	4212	3112
Medaka Yap1b	3792	2882
Zebrafish Yap1	7553	5427
Zebrafish Taz	8608	5230

enriched motifs using DREME returned different results when zebrafish Yap1 and Taz peaks were compared. Zebrafish Yap1 peaks showed enrichment in a series of known motifs similar to that of the medaka paralogs, including TEAD (as the second top hit: DREME E-value 7.4×10^{-147}), and also FOX, SOX, TP63 and POU (Fig. S10A). However, the collection of DNA-binding motifs associated with zebrafish Taz peaks seemed more divergent, with TEAD being only the 22nd best ranked motif (DREME E-value 9.5×10^{-3}) (Fig. S10B). This observation may simply suggest divergent cis-regulatory properties for zebrafish Taz. Alternatively, the disparities observed could be attributed to an incomplete detection of TEAD motifs by DREME, owing to small differences in the consensus sequence. To explore this possibility, we scanned the Yap family protein peaks imposing a consensus TEAD motif using AME. Using this approach, we could detect a very significant enrichment of the TEAD motif in the sets of peaks associated with all Yap family proteins, including zebrafish Taz (Fig. 4D).

To further characterize the chromatin regions targeted by Yap family proteins, we examined the co-occurrence of Yap-associated motifs identified in previous enrichment analyses (Table S2) using FIMO (Grant et al., 2011). Significant interactions among motifs were represented as a Cytoscape network (Shannon et al., 2003). The comparative analysis of these interaction networks revealed a very similar topology (i.e. connectivity between nodes) for motifs associated with medaka Yap1 and Yap1b, with TEAD1, RUNX1, AP1, SMAD, SOX10, FOXD3 and POU5F1 being among the most interconnected nodes (Fig. S11A,B). In contrast, zebrafish Yap1 and Taz showed a more divergent network topology, but some of the nodes, such as POU5F1, FOXD3 and AP1, still displayed a dominant weight in both networks (Fig. S11C,D). This is in agreement with the observation that the overlap between medaka Yap1 and Yap1b peaks is larger than that of zebrafish Yap1 and Taz (Fig. S9A,B).

To examine the collection of genes potentially targeted by Yap family proteins, we associated each peak to the closest TSS. As previously detected for the DamID peaks themselves, we observed that a large fraction of the Yap1b target genes (71%) were also associated with Yap1 in medaka. However, the proportion of genes potentially co-regulated by Taz and Yap1 was smaller (43%) in zebrafish (Table 1, Fig. S9G,H). Our observations are in line with the conservation of the Tead-binding domain between Yap1 and Yap1b (Fig. S3), and indicate that, despite the Yap1b divergent transactivation domain, both medaka paralogs target a largely overlapping set of genes. To gain insight into the attributes of these genes, we used Panther (Mi et al., 2017) to investigate statistically overrepresented gene ontology (GO) terms. When GO terms from the categories 'molecular function' and 'protein class' were examined, a similar set of enriched terms was obtained for genes targeted by Yap1, by Yap1b or by both, including 'transmembrane receptor tyrosine kinase activity' and 'transcription factor activity' as the most significant terms (Table 2, Table S3). Regarding GO terms linked to the 'Biological process' category, this list included terms such as:

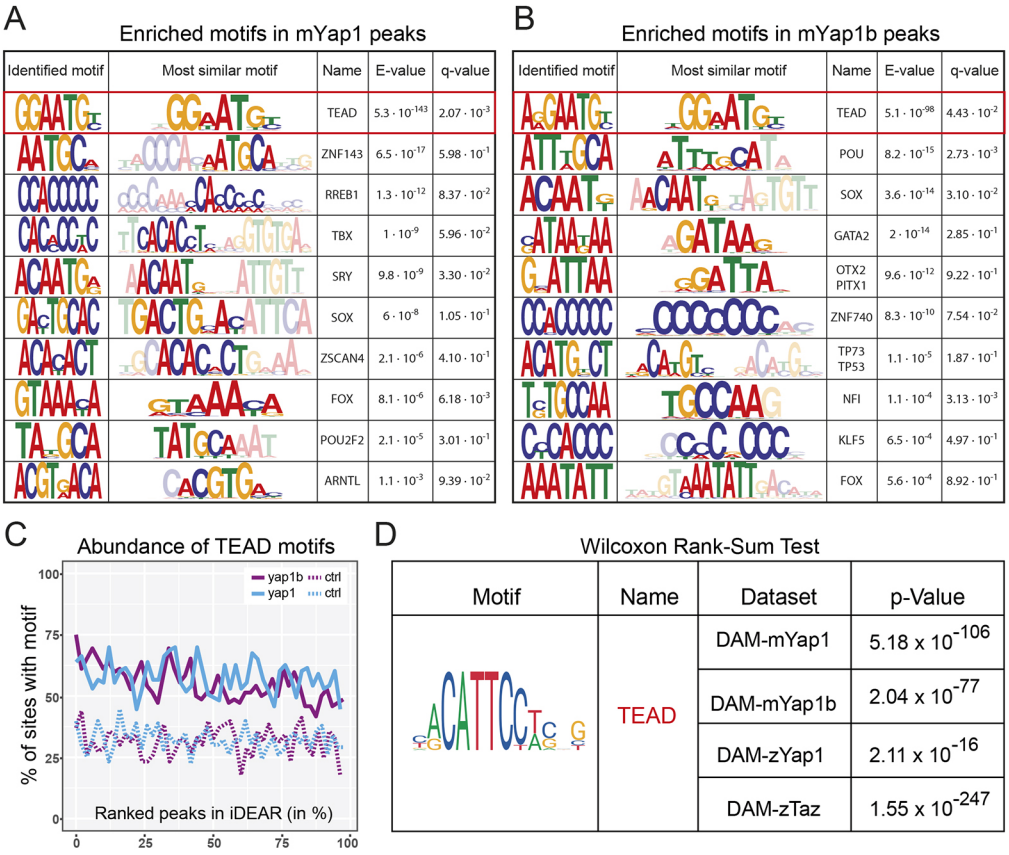

Fig. 4. Analysis of motifs enriched in medaka DamID-seq peaks. (A,B) List of enriched motifs associated with medaka Yap1 (A) and Yap1b (B) peaks, as identified by DREME and recognized by Tomtom. Both DREME E-value and Tomtom q-values are shown. The TEAD motif is highlighted with red boxes. (C) The abundance of TEAD motifs in relation to their iDEAR ranking is shown for positive and negative peaks. (D) AME analysis shows a significant enrichment for the TEAD motif in each of the different DamID-seq datasets.

Development (2019) 146, dev173286. doi:10.1242/dev.173286

Table 2. Over-represented GO-slim terms associated with genes targeted both by Yap1 and Yap1b

	Fold enrichment	Raw *P* value	FDR
PANTHER GO-slim biological process			
Negative regulation of apoptotic process	2.66	6.35E-06	7.59E-04
Transmembrane receptor protein serine/threonine kinase signaling pathway	2.58	1.05E-03	2.79E-02
Embryo development	2.28	6.34E-04	2.16E-02
Ectoderm development	2.02	3.64E-05	2.17E-03
Transmembrane receptor protein tyrosine kinase signaling pathway	1.95	1.34E-03	3.21E-02
Regulation of cell cycle	1.86	2.09E-03	4.55E-02
MAPK cascade	1.76	1.84E-04	7.34E-03
Cell differentiation	1.74	6.73E-06	5.36E-04
Regulation of phosphate metabolic process	1.59	1.30E-04	6.23E-03
PANTHER GO-slim molecular function			
Sequence-specific DNA binding transcription factor activity	1.36	5.26E-04	4.92E-02
PANTHER protein class			
Transcription factor	1.52	7.52E-07	1.62E-04

The table shows fold enrichment, *P* and FDR values for the categories Biological Process, Molecular function and Protein Class. Statistical significance was determined using the Fisher's Exact test with FDR multiple test correction.

'negative regulation of apoptotic process', 'embryo development', 'cell differentiation' and 'regulation of cell cycle', which are consistent with the reported roles for Yap family members in differentiation, proliferation and cell survival (Piccolo et al., 2014). This finding, together with the observation of Yap1 and Yap1b binding to well-known targets of the Hippo pathway in mammals (Fig. 3A, Fig. S8) suggests shared features in the transcriptional program controlled by Yap proteins across vertebrates. To investigate the extent to which this program is conserved, we compared the overlap between the lists of genes we identified as Yap family targets by DamID-seq, with genes identified as targets in previous ChIP-seq studies using mammalian cells (Estarás et al., 2017; Lian et al., 2010; Zanconato et al., 2015). The overlap between these gene lists is statistically very significant in all cases (Fig. S12A). Thus, ∼25% of the genes identified in each our four DamID-seq experiments are also present in at least three out of the six ChIP-seq datasets considered. Furthermore, a few hundred genes, ∼10% of those identified by DamID-seq, are included in five or six of the ChIP-seq datasets (Fig. S12B, Table S6). This group comprises many known transcriptional targets of Yap/Tead complexes, such as *ajuba*, *amotl2a*, *arhgef7a*, *ccnd2a*, *ctgf*, *cyr61*, *lats2*, *smad6b* or *tead1b* (Dataset S2). This observation indicates that, despite the different cell types, developmental stages, paralogs and even species considered, a substantial part of the gene battery controlled by Yap family proteins is conserved across vertebrates.

yap1b mutant alleles enhance *yap1*$^{-/-}$ developmental defects during early embryogenesis in medaka

Our DamID-seq analysis indicated that the identified paralog Yap1b targeted a similar collection of genes through a largely overlapping set of cis-regulatory elements. This may suggest that, in spite of its divergent C-terminal activation domain, Yap1b plays a cooperative role, together with Yap1, in transcriptional regulation. Alternatively, Yap1b could act as a dominant-negative form of Yap1 if the atypical transactivation domain was unable to recruit the Pol II complex. To distinguish between these possibilities and to further understand the role of Yap1b, we generated CRISPR-mediated targeted mutations at the exon2 of medaka *yap1b*. Two different alleles, y*ap1bΔ136pb* and *yap1bΔ84pb*, were identified and maintained as stable lines. These harbor chromosomal lesions that consist of exon 2 deletions of 136 and 84 bp (Fig. 5A). The first, *yap1bΔ136pb*, results in a frameshift mutation and a premature stop codon within the Tead-binding domain of the protein; the second, *yap1bΔ84pb*, in a 28 amino acid deletion of the Tead-binding domain (Fig. 5B). Despite both alleles being predicted to be null mutations, *yap1b*$^{-/-}$ embryos developed normally and could not be distinguished from their wild-type siblings (Fig. 5C-H). In fact, fish survival and fertility were not affected in adult *yap1b*$^{-/-}$ mutants. This result excluded the possibility of *yap1b* playing an obvious non-redundant role during embryogenesis and tissue maintenance. To investigate whether the gene may have a cooperative role with its paralog *yap1b*, we crossed double heterozygous fish, *yap1*$^{+/-}$*; yap1b*$^{+/-}$, and examined the phenotype and genotype of their progeny. These analyses showed a negative epistatic interaction between both genes. Thus, the phenotypic malformations observed in *yap1*$^{-/-}$ mutants (i.e. optic cup flattening, delayed blastopore closure and increased cell death) appeared enhanced in *yap1*$^{-/-}$*; yap1b*$^{+/-}$ embryos, and were even more evident in *yap1*$^{-/-}$*; yap1b*$^{-/-}$ double mutants (Fig. 6A-D). Quantitative measurements in wild type, single and double mutants at stage 20 confirmed an increased optic cup deformity, tissue flattening, embryo axis shortening and delayed blastopore closure in double mutants (Fig. S13). Bright-field microscope examination of double mutants also revealed signs of increased cell death from stage 20-21 onwards. To explore this possibility, we analyzed caspase 3 levels in stage 20 embryos collected from a *yap1*$^{+/-}$*;yap1b*$^{+/-}$ cross (Fig. 6E-L). These stainings confirmed a significant and progressive increase in the number of apoptotic cells in *yap1*$^{-/-}$ embryos when additional copies of *yap1b* are mutated (Fig. 6Q). In contrast, similar levels of apoptosis were observed in embryos harboring at least one wild-type allele of *yap1* (Fig. S14). In fact, no morphological malformations were observed in these embryos, suggesting that a single copy of *yap1* is sufficient for a complete phenotypic rescue. Finally, we examined the impact of *yap1* and *yap1b* mutations on the mitotic index, as determined by pH3 staining in stage 20 embryos (Fig. 6M-P). In spite of the known role of Yap proteins in the control of growth and cell proliferation (Huang et al., 2005), we could not detect any significant difference in the number of mitotic cells per area (Fig. 6R). This finding indicates that, at least in the context of early developing embryos, Yap paralogs do not play a significant role in the control of cell proliferation.

Taken together, our results suggest that, although *yap1* and *yap1b* cooperate in regulating cell survival and tissue morphogenesis, *yap1* has a dominant role due to the reduced zygotic levels of *yap1b*. To confirm this dominance, and validate our DamID-seq analysis, we examined using qPCR the relative levels of a number of genes directly targeted by Yap family proteins (including *yap1* and *yap1b*) in wild-type and single mutant embryos at stage 16 (Fig. 7A). We

Development (2019) 146, dev173286. doi:10.1242/dev.173286

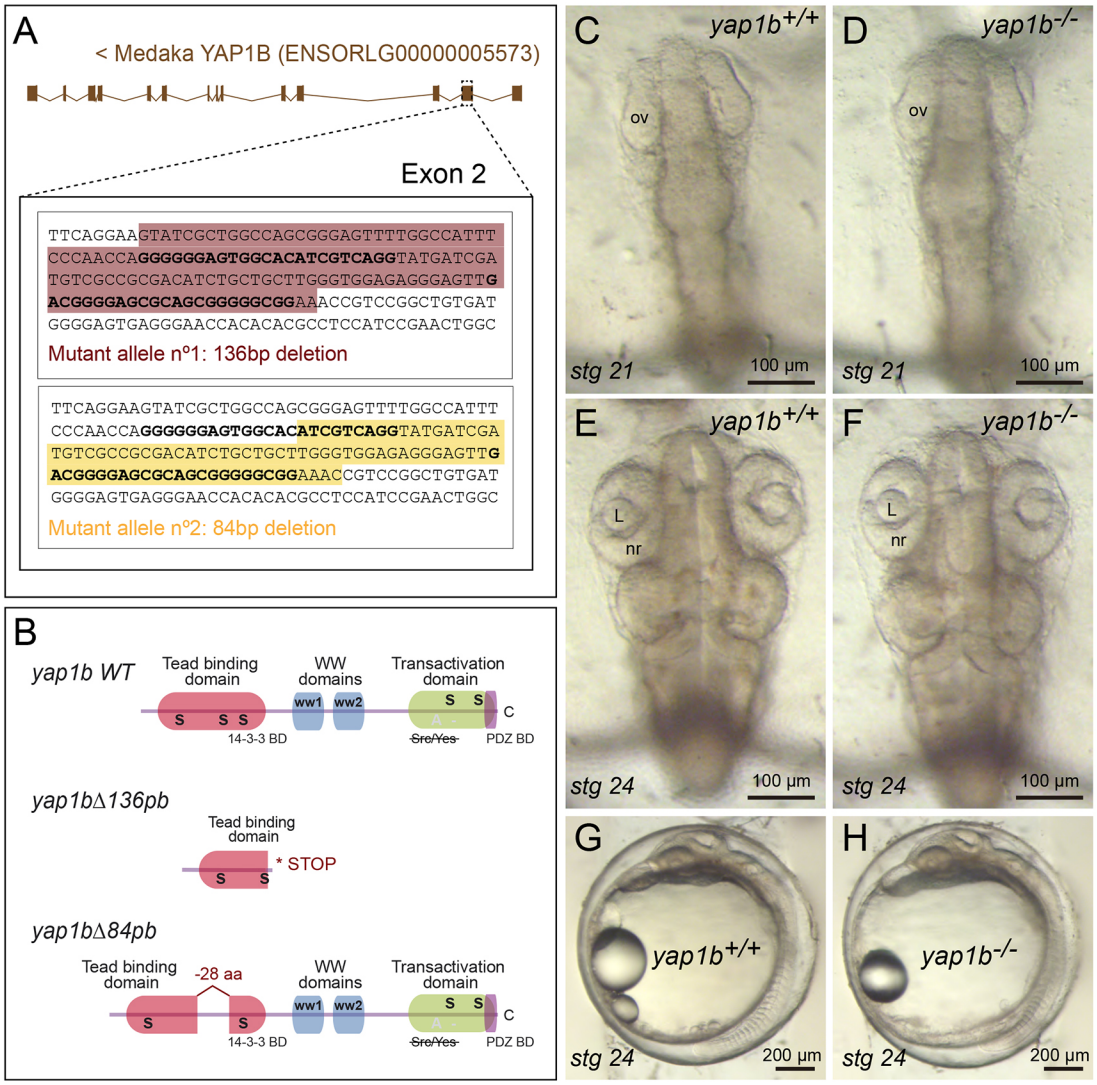

Fig. 5. Generation of *yap1b* mutant alleles by CRISPR/Cas9 genome editing. (A) Schematic representation of the 136 bp and 84 bp deletions (shadowed sequence) generated in exon 2 of *yap1b* in medaka (see Materials and Methods). (B) The predicted Yap1b protein structure is depicted for the wild-type and mutant proteins. The *yap1bΔ136pb* deletion results in a frameshift mutation and premature stop codon, whereas *yap1bΔ84pb* results in a 28 amino acid deletion of the TEAD-binding domain. No phenotypic differences were observed when comparing wild-type (C,E,G) and *yap1b* mutant embryos (D,F,H) at stages 21 (C,D) and 24 (E-H). ov, optic vesicle; L, lens; nr, neural retina.

found significantly reduced levels for all targeted genes tested in *yap1* mutants, and milder reductions in *yap1b*$^{-/-}$ embryos (Fig. 7A). To further confirm our dominance hypothesis, we injected *yap1b* mRNA into one-cell stage *yap1*$^{-/-}$ mutant embryos. Remarkably, the severe malformations exhibited by *yap1*$^{-/-}$ mutants were partially (30%) or completely (70%) rescued by *yap1b* injection (Fig. 7B-E). Thus, despite the divergent architecture of the Yap1b transactivation domain, the protein seems to be transcriptionally active and can replace Yap1 function, at least in a developmental context.

DISCUSSION

Yap family proteins and Tead factors have been shown to work as a functional tandem, as Yap proteins cannot interact directly with the genome, and the function of Tead regulators depends on the ability of the Yap/Taz C-terminal activation domain to recruit the Pol II complex (Galli et al., 2015; Stein et al., 2015; Vassilev et al., 2001; Zanconato et al., 2015). The bipartite nature of the Yap/Tead transcriptional couple is well illustrated by classical experiments overexpressing Yap in lymphocytic cells, which resulted in a 300-fold induction of Tead activity (Vassilev et al., 2001). The identification in this study of Yap1b, a novel Yap paralog with a transcriptional activation domain very divergent from those previously described for Yap1 (Sudol, 1994) and Taz/Wwtr1 (Kanai et al., 2000), raised questions about its evolutionary origin, chromatin-binding properties and biological function.

Evolution of Yap family proteins in teleosts

Our phylogenetic analyses have outlined an evolutionary sequence for the emergence and radiation of Yap family paralogs in teleosts. Previous studies had shown that Yap emerged in metazoans as a novel Tead partner, and duplicated to give rise to the paralogs Yap and Taz in the vertebrate lineage (Hilman and Gat, 2011). Both paralogs share a common domain architecture and a particular feature, which appears to be a vertebrate-specific acquisition: the capacity of being activated by kinases of the Src family at their C-terminal activation domain (Elbediwy and Thompson, 2018; Sudol, 1994). Here, we show that, during the teleost-specific

Development (2019) 146, dev173286. doi:10.1242/dev.173286

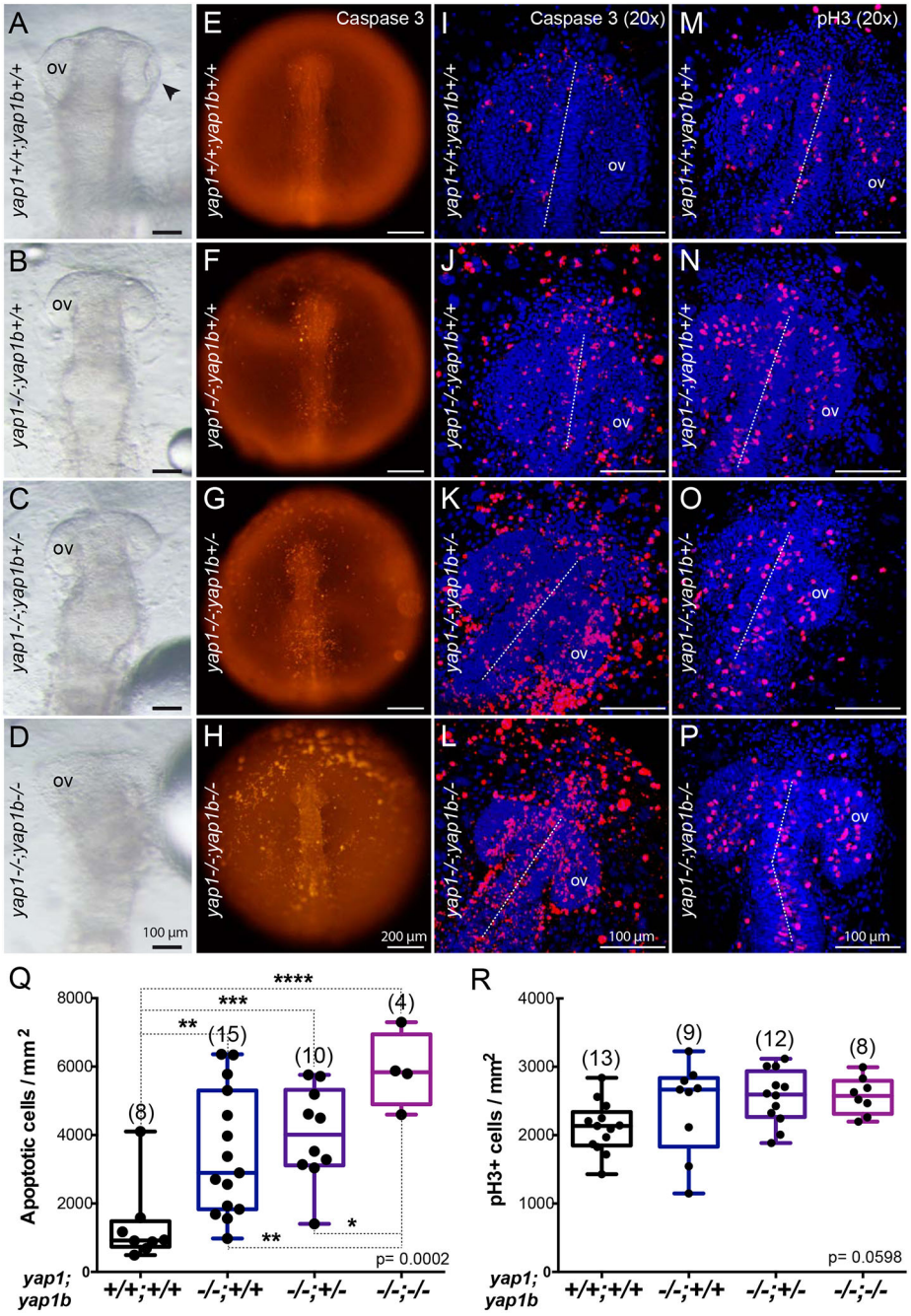

Fig. 6. *yap1* and *yap1b* cooperate in regulating cell survival and tissue morphogenesis. Bright-field images of the anterior half of *yap1*$^{+/+}$;*yap1b*$^{+/+}$ (A), *yap1*$^{-/-}$;*yap1b*$^{+/+}$ (B), *yap1*$^{-/-}$;*yap1b*$^{+/-}$ (C) and *yap1*$^{-/-}$;*yap1b*$^{-/-}$ (D) stage 21 embryos from a double heterozygous cross showing negative epistatic interaction between *yap1* and *yap1b*. *yap1*$^{-/-}$ enhanced malformations in *yap1*$^{-/-}$;*yap1b*$^{-/-}$ double mutants (D). Caspase 3 staining reveals apoptotic cells in stage 20 *yap1*$^{+/+}$;*yap1b*$^{+/+}$ (E,I), *yap1*$^{-/-}$;*yap1b*$^{+/+}$ (F,J), *yap1*$^{-/-}$;*yap1b*$^{+/-}$ (G,K) and *yap1*$^{-/-}$;*yap1b*$^{-/-}$ embryos (H,L). Whole embryos are shown under the fluorescent stereo microscope (E-H). DAPI counterstained confocal images show individual apoptotic cells (I-L). DAPI counterstained confocal images of pH3-positive mitotic cells in stage 20 *yap1*$^{+/+}$;*yap1b*$^{+/+}$ (M), *yap1*$^{-/-}$;*yap1b*$^{+/+}$ (N), *yap1*$^{-/-}$;*yap1b*$^{+/-}$ (O) and *yap1*$^{-/-}$;*yap1b*$^{-/-}$ embryos (P). Quantification of caspase 3-positive cells per area shows a significantly increased apoptosis with fewer functional copies available of the Yap paralogs (Q). Quantification of pH3-positive cells per area shows not significant differences in mutants for the Yap paralogs (R). Boxes represent the quartiles; the whiskers indicate the the maximum and minimum values. One-way ANOVA analysis followed by Fisher's LSD test was used to evaluate statistical significance. ov, optic vesicle. ****P<0.0001; ***P<0.001; **P<0.01; *P<0.05.

whole-genome duplication event, the two ancient paralog genes duplicated again to generate four functional copies, *yap1*, *yap1b*, *taza* and *tazb*. In fact, we show that these four paralogs are present in extant species of basal teleost groups, such us Elopomorpha (eel) and Osteoglosomorpha (elephantfish). Regarding *taz* paralogs, further evolution in the teleost lineage resulted in the subsequent elimination of one copy before the Otomorpha radiation, and of the second copy in Percomorpha. This finding implies that one in every four vertebrate species (i.e. the whole Percomorpha clade) does not harbor any functional copy of *taz* in their genomes. The evolutionary history of *yap* paralogs was quite different. First, *yap1* diverged very little from the ancestral gene and became the functionally dominant paralog in teleosts (Kimelman et al., 2017; Miesfeld et al., 2015; Porazinski et al., 2015). In contrast, *yap1b* was lost in Otomorpha (e.g. zebrafish) and its transcriptional activation domain was substantially modified in euteleosts (e.g. medaka), eliminating the characteristic tyrosine residues that can be phosphorylated by Src. The elimination of these residues should affect a major Hippo-independent regulatory input on the protein, as SFK-mediated phosphorylation has been proved to be essential for the transcriptional activity of Yap/Tead complexes (Calvo et al., 2013; Li et al., 2016). In fact, the modification of Yap1b C-terminal domain is deep enough to raise the question of whether its transactivation properties are impaired. Provided that the Yap1b Tead-binding domain is well conserved and seems functional according to our DamID data, a transcriptionally inactive C-terminal domain could be compatible with a dominant-negative function for Yap1b. Our genetic data strongly argue against this possibility, as *yap1b* loss of function does not alleviate but rather intensifies the phenotypic consequences of *yap1* mutation. The most likely

Development (2019) 146, dev173286. doi:10.1242/dev.173286

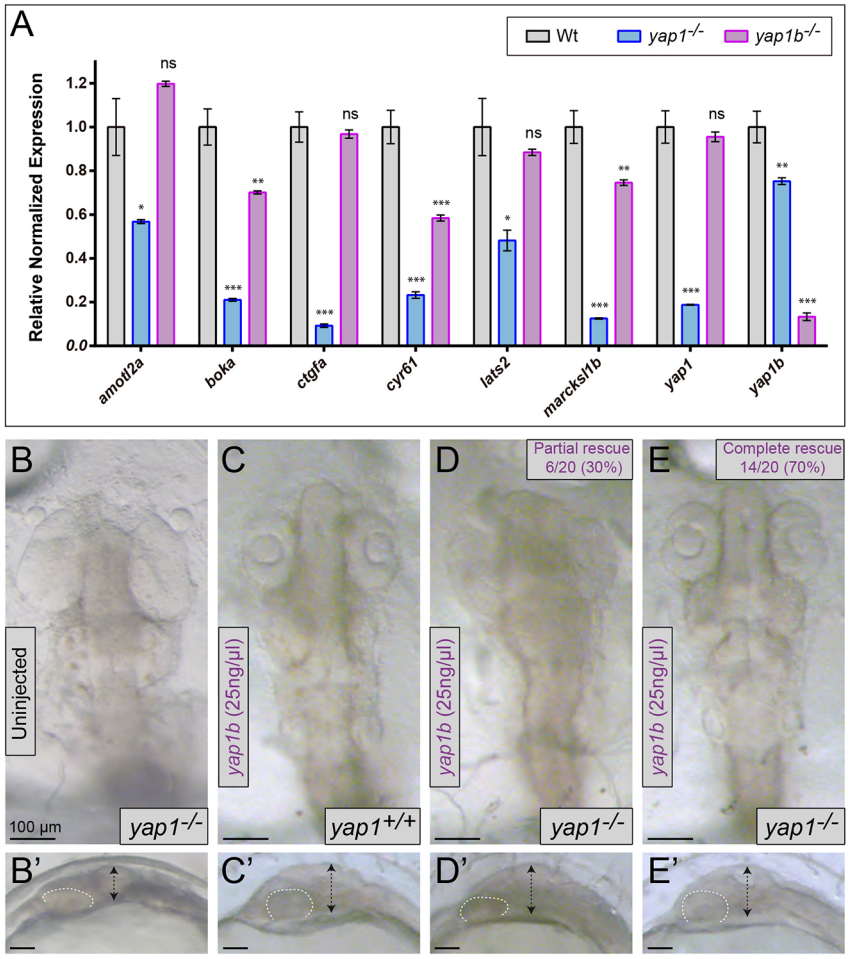

Fig. 7. *yap1*/*yap1b* relative regulatory weight and *yap1b* rescuing capacity. (A) Quantification of the expression levels of genes targeted by Yap family proteins in wild-type, $yap1^{-/-}$ and $yap1b^{-/-}$ medaka embryos (stage 16) by qPCR (n=3). Comparative dorsal (B-E) and lateral (B′-E′) views of stage 24 medaka embryos in *yap1b* rescuing experiments. Embryo genotype (either $yap1^{+/+}$ or $yap1^{-/-}$) and *yap1b* injections are indicated. Embryo flattening (double-headed arrows) and optic cup shape (dotted lines) are also highlighted. The complete $yap1^{-/-}$ phenotypic rescue upon *yap1b* mRNA injection (E). One-way ANOVA analysis followed by Fisher's LSD test was used to evaluate statistical significance. ***P<0.001; **P<0.01; *P<0.05; ns, not significant.

hypothesis therefore is that Yap1b transcriptional activation domain, in contrast to that of other vertebrate paralogs, does not depend on SFK-mediated activation. This was further confirmed by the ability of *yap1b* to rescue *yap1* mutation when injected as mRNA. Yap1b regulatory properties would then be similar to those of invertebrate Yap proteins that are not regulated by kinases of the Src family, as is the case for Yorkie in *Drosophila* (Elbediwy and Thompson, 2018).

Genome-wide analysis of chromatin binding in Yap family proteins

The recruitment of the vertebrate Yap or Taz, or their co-factor Tead, to the chromatin has been previously investigated in genome-wide ChIP-seq studies performed either in mammalian ESCs (Estarás et al., 2017; Lian et al., 2010), cancer cell lines (Galli et al., 2015; Nardone et al., 2017; Stein et al., 2015; Zanconato et al., 2015) or embryonic tissues (Cebola et al., 2015; Lin et al., 2017). Although there are some discrepancies regarding the number of targeted regions (i.e. ranging from 1000 to 7000 peaks), most if not all of these works converged in the identification of a large overlap between Tead and Yap/Taz binding, and succeeded in revealing Tead as the most enriched motif in Yap/Taz peaks. Furthermore, these studies consistently identify a number of genes, including *Amotl2*, *Ctgf*, *Cyr61* or *Ajuba*, as direct transcriptional targets. Here, we have used DamID-seq to characterize the binding of Yap paralogs to the genome in zebrafish and medaka gastrulating embryos. This approach allows us to bypass two important limitations of ChIP-seq studies: the dependency on ChIP-grade antibodies (which may not recognize the teleost proteins) and the need for a large number of sample cells. The latter requirement, in particular, may have prevented chromatin occupation analyses at early stages of development in vertebrates. DamID-seq has been used as a standardized protocol for *in vivo* chromatin profiling in *Drosophila* (Marshall and Brand, 2017; Marshall et al., 2016; Southall et al., 2013) and, more recently, once toxicity issues were experimentally resolved, in medaka (Gutierrez-Triana et al., 2016) and mammals (Cheetham et al., 2018; Tosti et al., 2018). Several lines of evidence indicate that our DamID-seq approach has succeeded in the identification of bona-fide binding sites for Yap paralogs during early embryogenesis. Our triplicated analyses show high reproducibility, and in all cases we could retrieve the Tead motif: either directly as the most-enriched motif using DREME (i.e. in medaka Yap1 and Yap1b DamID-seq experiments) or after imposing a consensus TEAD motif using AME (i.e. in zebrafish experiments for Yap1 and Taz). In addition, besides TEAD, we could identify a significant enrichment for some known motifs associated with transcriptional regulators reported to interact with Yap proteins, such as those of p63, p73 and Tbx5 (Piccolo et al., 2014). Furthermore, the identified marks, which partially overlap with open chromatin regions, can be found in the vicinity, if not directly in the promoter, of 'beacon' genes, such as *ctgf*, *cyr61*, *amotl2*, *lats2*, *ajuba* or *ccne1*, which have been proved to be direct transcriptional targets of Yap/Tead complexes in this and previous studies (Lin et al., 2017; Stein et al., 2015; Zanconato et al., 2015).

Our DamID-seq studies have allowed us to characterize the DNA-binding properties of the newly identified paralog Yap1b. As

Development (2019) 146, dev173286. doi:10.1242/dev.173286

already anticipated by the sequence conservation of its Tead-binding domain, Yap1b targets a set of chromatin regions that largely overlaps those occupied by Yap1. Moreover, our comparative analyses provide a reference resource to investigate the genetic program controlled by the different co-regulators of the Yap family during early embryogenesis in vertebrates. The comparison between our results and previous ChIP-seq analyses suggests that a substantial part of the transcriptional program controlled by Yap proteins is conserved in vertebrates, regardless of the cell type and developmental stage considered. Further analyses will be required to systematically investigate gene regulatory commonalities versus tissue- and stage-specific adaptations.

Cooperative role of yap paralogs during early development in teleost species

One of the main motivations of this work arose from the phenotypic discrepancies observed between *yap1* mutants in medaka and zebrafish. The mutation of *yap1* in medaka results in strong malformations, which affect the development of many organ rudiments, including the heart, eye, brain and somites at segmentation stages (Porazinski et al., 2015). In contrast, the equivalent *yap1* mutation in zebrafish only causes very mild defects. Strong embryonic malformations, similar to those observed in medaka *yap1* mutants, are only obtained after the simultaneously mutation of *yap1* and *taz* in zebrafish (Kimelman et al., 2017; Miesfeld et al., 2015). The analysis of these phenotypic discrepancies lead us to the finding that the second paralog present in the medaka genome, and in other euteleosts, was not *taz*, as previously assumed (Porazinski et al., 2015), but *yap1b*: a newly identified paralog of the *yap* family. Comparative analysis of the expression profiles of *yap* paralogs in zebrafish and medaka provides an explanation of the phenotypic differences observed upon *yap1* mutation. Whereas *yap1* and *taz* are expressed at similar levels during gastrulation and somitogenesis in zebrafish, low *yap1b* levels are detected during this window in medaka. Our observations suggest that paralog compensation by *taz* mitigates *yap1* loss of function in zebrafish but not in medaka, where *yap1* plays a more dominating role. Interestingly, the maternal contribution of *yap1b* is three times more than that of *yap1*. As Yap has been shown to play a key role in the activation of the early zygotic genome in mice (Yu et al., 2016), this result- may suggest an important role for Yap1b in maternal-to-zygotic transition in medaka. However, loss of maternal *yap1b* has no apparent phenotypic consequences, as medaka mutants are fertile and produce a normal offspring. Further studies need to be conducted to determine whether blocking the maternal contribution of *yap1* and *yap1b* simultaneously will have any consequence on zygotic activation in medaka embryos.

Despite the absence of overt phenotypes in *yap1b* mutant embryos, the phenotypic analysis of $yap1^{-/-};yap1b^{-/-}$ double mutants in medaka revealed important roles for Yap1b in the regulation of tissue morphogenesis and cell survival during early embryogenesis. These functions are consistent with our GO-terms analysis for Yap1 and Yap1b target genes, which yielded terms such as ‘negative regulation of apoptotic process’ and ‘embryo development’, and with previously reported roles for Yap paralogs during embryogenesis in teleost (Kimelman et al., 2017; Porazinski et al., 2015). Interestingly, *yap1b* cooperative role does not depend on SFK-mediated activation. The physiological role of Yap phosphorylation at its transcriptional activation domain is still not well understood, either during embryogenesis or in adult tissues. However, SFK-mediated activation of Yap has been shown to be crucial for liver and intestinal mucosa regeneration (Taniguchi et al., 2015). The particular paralogs composition in euteleosts, with a single SFK-dependent protein, provides now a unique opportunity to further investigate the role of this regulatory input in developing and adult tissues.

The phylogenetic analysis of the Yap family in teleosts uncovered Yap1b, a new paralog protein with an atypical transcriptional activation domain, which cannot be phosphorylated by Src-related kinases. By applying a DamID-seq approach to gastrulating embryos, we could characterize the binding properties not only of Yap1b but also of all the other paralogs present in medaka and zebrafish. These analyses constitute a reference resource to investigate chromatin occupation by Yap family proteins during early embryogenesis in vertebrates, and specifically indicate that medaka Yap1 and Yap1b share similar chromatin-binding properties. Despite the divergent transcriptional activation domain of Yap1b, the phenotypic analysis of *yap1* and *yap1b* medaka mutants reveals functional overlap of both paralogs. Our data show that *yap1* and *yap1b* cooperatively regulate cell death and tissue morphogenesis during early embryogenesis.

MATERIALS AND METHODS

Fish maintenance

The zebrafish (*Danio rerio*) *AB/Tübingen* (AB/TU) and medaka (*Oryzias latipes*) iCab wild-type strains were maintained under previously described experimental conditions (Iwamatsu, 2004; Kimmel et al., 1995). All animal experiments were carried out according to the guidelines of our Institutional Animal Ethics Committee.

Phylogenetic analysis and genome browsing of yap family genes

Proteins of the Yap family were aligned using MAFFT as implemented in T-Rex (Boc et al., 2012). Maximum likelihood trees were inferred with PHYML software under a WAG +G model using 100 bootstrap replicates (Boc et al., 2012). To retrieve protein sequences and to reconstruct gene arrangement in the vicinity of Yap family members, we used genome annotations available in NCBI (www.ncbi.nlm.nih.gov/genome/), UCSC (genome.ucsc.edu/) and Ensembl (www.ensembl.org/index.html). The following genome assembly versions were used: *Anguilla japonica* (Japanese eel) Ajaponica_ver_D2; *Astyanax mexicanus* (Pachón cavefish) 2.0; *Clupea harengus* (Atlantic herring) ASM96633v1; *Danio rerio* (Zebrafish) Zv9; *Esox lucius* (Northern pike) EsoLuc1.0; *Gadus morhua* (Atlantic cod) gadMor1; *Gasterosteus aculeatus* (Stickleback) BROAD_S1; *Homo sapiens* (Human) hg38; *Lepisosteus oculatus* (Spotted gar) LepOcu1; *Mus musculus* (Mouse) m38; *Oreochromis niloticus* (Tilapia) Orenil1.0; *Oryzias latipes* (Medaka) v1.0; and *Paramormyrops kingsleyae* (Elephantfish) Pkings_v0.1.

Generation of medaka CRISPR lines

Generation of yap1 mutants

Three sgRNAs were designed against exon 2 of the medaka *yap1* gene (ENSORLG00000002708) using the CCTop online tool (Stemmer et al., 2015). Designed primers (Table S4) were hybridized to generate dimers that were inserted into pDR274 plasmids (Addgene, #42250). Resulting vectors were linearized with HindIII and purified by column (GFX PCR DNA and Gel Band purification Kit, G&E). sgRNA molecules without cap and poly(A) tail were generated using the T7 MAXIscript kit (Ambion). To produce Cas9 mRNA, pCS2-nCas9n plasmid (Addgene, #47929) was linearized using NotI, column purified and transcribed (SP6 mMessage mMachine Kit, Ambion). Transcribed sgRNAs were treated with DNAseI to remove the DNA template, precipitated by adding lithium chloride and ethanol, cleaned up (RNA cleanup Kit, Qiagen) and resuspended in nuclease-free water. An ~5 nl of a mix of Cas9 mRNA at 300 ng/µl and the three sgRNAs produced each were injected at 40 ng/µl into one-cell stage medaka embryos. Founders were identified by genotyping fertilized F1 embryos using a T7 endonuclease assay (Table S4). To identify the specific mutant allele of each F1 adult fish, the affected genomic region was amplified using the Advantage 2 PCR Kit (Clontech), cloned into pSpark vectors (Canvax Biotech) and sequenced. *yap1Δ7pb* and *yap1Δ11pb* mutant embryos can be genotyped through PCR and digestion with MspI and TfiI restriction enzymes, respectively.

Development (2019) 146, dev173286. doi:10.1242/dev.173286

Generation of a *yap1b* mutant line in medaka

Two sgRNAs were designed against medaka *yap1b* (ENSORLG00000005573) exon 2 using CRISPRScan (Moreno-Mateos et al., 2015). For each target, a 52 nt oligo including a T7 promoter followed by the CRISPR-binding site without the PAM sequence (Table S4) were annealed against a universal reverse 80 nt oligo to generate a 117 bp DNA duplex by PCR. Each DNA duplex was purified by column and transcribed to generate sgRNAs using the MAXIscript T7 Transcription kit (Ambion). sgRNAs were injected and mutant alleles identified as described in the previous section. *yap1bΔ136pb* and *yap1bΔ84pb* mutants can be genotyped by PCR (Table S4).

Rescue experiments

To rescue *yap1* mutation, *yap1b* mRNA was synthesized using the SP6 mMessage mMachine kit (Ambion) and injected into one-cell stage medaka at 25 ng/µl.

iDamID-seq

Library preparation

For iDamID-seq experiments and posterior bioinformatics analysis, we followed the protocol reported for medaka (Gutierrez-Triana et al., 2016) (see also Fig. S5). Zebrafish *yap1* (ENSDARG00000068401) and taz/*wwtr1* (ENSDARG00000067719), as well as medaka *yap1*- and *yap1b*-coding sequences were cloned into pCS2+::cMyc-oDam-FL-GFP-NLS, by replacing the GFP-NLS sequence (Table S4). mRNAs for each DAM-TF cassette were synthesized using the SP6 mMessage mMachine kit (Ambion) and injected into one-cell stage medaka at 10 ng/µl and into zebrafish embryos at 50 ng/µl. Forty embryos were used in each independent DamID replicate. After injection, gDNA was extracted, either from 80%-epiboly zebrafish (8 hpf) embryos or stage 16 medaka embryos, and fragmented using DpnII (NEB). DNA was subsequently dephosphorylated with alkaline phosphatase (NEB) and digested with DpnI to cleave specifically GATC methylated sites. Adapters, produced after hybridizing two oligos (Table S4), were ligated to both ends for each fragment to build up DNA libraries through a 25-cycle PCR amplification step using a phosphorothioate primer (Table S4). Each PCR product was run on a 1% agarose gel to check for the presence of a smear in DpnI-treated samples. Each library was then amplified five times before deep sequencing (Illumina HiSeq 2500 sequencing). Remaining DNA templates were removed with T7 exonuclease before sequencing. Three replicates for each sample were used for the iDamID-seq analysis.

Alignment and Identification of enriched sequences

Raw sequencing data was pre-processed using the Cutadapt tool to discard short reads (-m 34 parameter) and the ones corresponding to the adaptors used for deep sequencing. Reads from zebrafish and medaka proteins were mapped against the *GRCz10/danRer10* and the *NIG/UT MEDAKA1/oryLat2* genome versions of each breed, respectively, using *Bowtie2*. Duplicated reads were removed using Samtools rmdup. The identification of enriched regions was carried out using the R package iDEAR, available at bitbucket.org/juanlmateo/idear (branch v0.2). Default parameters were applied to the analysis.

Association of DamID peaks to neighbor genes and chromatin open regions

We assigned each DamID peak to its nearest gene using bedtools closest. The position of the transcription start site (TSS) of each gene was obtained from ENSEMBL database (Version 89) using the online tool Biomart (www.ensembl.org/biomart). To examine the percentage of peaks overlapping with open chromatin regions, their coordinates were compared with those from ATAC-seq peaks using *bedtools intersect.* As the zebrafish ATAC-seq data were mapped to an older genome version (danRer7), they had to be converted to the current version using LiftOver.

Motif enrichment analysis

DREME (Bailey, 2011) was used to identify predefined motifs in the complete set of specific peaks for the four examined proteins (-p parameter) with respect to their corresponding DAM-GFP control peaks (-n parameter). To ensure the statistical significance of this analysis, the set of control peaks were processed to have the same length distribution. To check for the presence of the TEAD motif from the JASPAR Database (MA0090.1) we used AME (McLeay and Bailey, 2010), applying a Mann–Whitney non-parametric test.

Analysis of motifs co-occurrence

FIMO (Grant et al., 2011) was used to scan the peak sequences for motifs either found in our enrichment analysis or previously associated with YAP/TAZ (Table S2). The motif hits found by FIMO were filtered to avoid motif overlap, discarding the motif with lowest significance if the overlap was for more than three bases. After this filtering, a PCA analysis was performed to identify the motifs in the four peaks sets that contribute the most. Next, for each pair of selected motifs, the proportion of peaks with at least one match for both motifs was calculated and this value was used a proxy for the degree of cooperation of both factors. Cytoscape (Shannon et al., 2003) was used to build networks representing the level of interaction between factors.

Overlap with ChIP-seq datasets

To obtain lists of genes associated with Yap1, Taz, or Tead binding in mammalian cells, we used the coordinates of the peaks available from different publications (Lian et al., 2010, Tables S1 and S2; Estarás et al., 2017, Table S2; Zanconato et al., 2015, YAP.narrowPeak and TAZ.narrowPeak). These coordinates were first converted to the assembly GRGh38 or GRGm38 using the Assembly Converter tool from www.ensembl.org. Using Biomart and the ENSEMBL database (Version 89), a protein-coding gene was assigned to each peak that was either overlapping its gene body or the closest to its TSS, within a limit of 50 kb for medaka, 100 kb for zebrafish or 200 kb for mouse or human, to account for the differences in genome length. The hypergeometric test was used to compute the significance of the overlap between the medaka- or zebrafish-associated genes and the genes associated with the ChIP-seq peaks.

Gene ontology analyses

Gene ontology analyses were performed using PANTHER (Mi et al., 2013). Only the GO terms identified with a False Discovery Rate lower than 0.05 using the PANTHER GO-Slim algorithm were taken into account.

YAP-family genes expression analysis

cDNA preparation

To check *yap1*, *taz* (*wwtr1*) and *yap1b* expression levels during pre-MBT, epiboly and phylotypic stages in teleosts, mRNA from medaka embryos at stages 7, 16 and 24, and from zebrafish embryos of 3, 8 and 24 hpf was obtained using TRIzol (Ambion). cDNA samples were obtained through retro-transcription using the iScript cDNA Synthesis kit (BioRad) and their concentration was measured in a Qubit fluorometer.

Whole-mount *in situ* hybridization

cDNA from medaka embryos at stage 24 was used to amplify part of the coding sequence of medaka *yap1* and *yap1b* genes. PCR products were cloned into pSC-A-amp/kan Strataclone plasmids (Agilent) to generate probes for whole-mount *in situ* hybridization experiments (Table S4). Probes were synthesized using digoxigenin-11-UTP nucleotides (Roche) and the T3 or the T7 polymerase (Roche) depending on the insert orientation. *In situ* hybridization was performed on fixed embryos at stage 15-16 following a previous protocol (Thisse and Thisse, 2008). Embryos were permeabilized using proteinase K for 4 min. Transcribed probes were used at a final concentration of 1 ng/µl. Embryos were washed with 0.05× SSC/PBS in decreasing salt concentrations.

qPCR and ddPCR

The expression levels of medaka *yap1* and *yap1b*, and zebrafish genes *yap1* and *taz* was quantified through RT-qPCR (CFX96 Touch Real-Time PCR Detection System) and normalized to the expression level of the housekeeping gene *ef1a* (Table S4). qPCR results were confirmed using the QX200 Droplet Digital PCR system (BioRad). Duplicated PCR reactions for each one of the tested genes were prepared using 15 ng of cDNA per reaction and following the manufacturer specifications. Every PCR reaction was atomized into a set of ∼22,000 1 nl drops using the QX200 Droplet Generator system. These droplets were transferred to 96-

well plates (#12001925, Bio-Rad). After the PCR, the relative amount of every amplified product was quantified using a QX200 Droplet Reader examining the fluorescence rate of each droplet. Reads were normalized to the levels of the housekeeping gene *ef1a*.

For qPCR experiments in mutant embryos, single embryos were homogenized in 1.0 ml of TRIzol (Invitrogen). DNA and RNA were extracted at the same time following the manufacturer's instructions. DNA was used for embryo genotyping. Total RNA was retro-transcribed with SuperScript IV VILO Master Mix (Thermo Fisher Scientific) and qPCR reactions were performed in triplicate using SsoAdvanced in a CFX98 real-time C1000 thermal cycler (Bio-Rad). Results were normalized with ef1a (for primer sequences, see Table S4).

Immunofluorescence assays

For the detection of apoptotic and mitotic cells, embryos collected from *yap1*$^{+/-}$;*yap1b*$^{+/-}$ adult fishes were fixed at stage 20 (5 somites) using PFA 4%. For YAP nuclear localization analysis, wild-type embryos were injected with the DamID-Yap1 and Yap1b cassette mRNA at the one-cell stage as described in the 'iDamID-seq' section, and fixed at stage 10 using 4% PFA. Fixed embryos were dechorionated with forceps, extensively washed with PBS-Tween 0.2% (PBT), treated with blocking solution (prepared with 10% fetal bovine serum) at room temperature for 2 h and incubated overnight at 4°C with the corresponding primary antibody diluted 1:500. Embryos were incubated with purified rabbit anti-active caspase-3 antibodies (BD Biosciences, 559565), rabbit anti-phospho-histone H3 antibodies (Merck Millipore, 06-570) or rabbit anti-c-Myc antibodies (Sigma-Aldrich, PLA0001). In the case of the c-Myc antibodies, 1% DMSO and 0.25% BSA were added to the blocking solution. Processed embryos were repeatedly washed with PBT and incubated overnight at 4°C in the dark with the Alexa Fluor 555 goat anti-rabbit antibody (diluted 1:500 (Thermo Fisher, A21429). Nuclei counterstaining was performed using DAPI (Sigma-Aldrich) diluted 1:1000 and phalloidin using phalloidin-Alexa488 (Invitrogen) diluted 1:20 and incubated in PBT overnight at 4°C.

Confocal microscopy and image processing

Selected embryos were mounted in 35 mm FluoroDish plates (*WPI*, *FD3510-100*) using 1% low melting agarose. These embryos were examined using confocal microscopy (Zeiss LSM 880) with 25× or 40× multi-immersion objectives. All pictures were processed using FIJI/ImageJ (Version 1.50i). For each image and channel (red and blue), a maximum projection was generated and the background noise was completely minimized (Subtract Background set at 200). For quantification of apoptotic and mitotic cells, masks were applied for both channels. The mask generated for the red channel was segmented using the Watershed algorithm. Only the regions marked with the primary antibody that also corresponded to nuclei with a 6-200 µm^2 area were considered to avoid debris. Apoptotic and pH3-positive cells were counted on the embryo surface and extrapolated to a section of 1 mm^2. Morphometric analysis of wild-type and mutant embryo structures at stage 20 was performed also using FIJI/ImageJ (Version 1.50i).

Statistical analysis

Quantitative data were evaluated using Prism 6.0 (GraphPad). The statistical analyses applied, *n* values and significance levels are indicated in figure legends.

Acknowledgements

We thank Nacho Maeso, Joaquin Letelier, Cristian Undurraga, Juan Tena and Rocío Polvillo for their critical input and/or their excellent technical assistance. We are grateful to Bryan Link and Joel Miesfeld for sharing zebrafish *yap* and *taz* mutants.

Competing interests

The authors declare no competing or financial interests.

Author contributions

Conceptualization: J.V.-M., M.A.-G., J.L.M., J.R.M.-M.; Methodology: J.V.-M., J.A.G.-T., M.A.-G., L.B., J.L.G.-S., J.L.M., J.W.; Validation: J.V.-M., J.A.G.-T., J.L.G.-S., J.L.M., J.W., J.R.M.-M.; Formal analysis: J.V.-M., M.A.-G., L.B., J.L.M., J.R.M.-M.; Investigation: J.V.-M., J.A.G.-T., M.A.-G., L.B., J.L.M., J.R.M.-M.; Resources: J.L.G.-S., J.R.M.-M.; Data curation: J.V.-M., J.A.G.-T., M.A.-G., J.L.M.; Writing - original draft: J.V.-M., J.R.M.-M.; Writing - review & editing: J.V.-M., M.A.-G., J.R.M.-M.; Visualization: J.V.-M., J.A.G.-T., J.L.G.-S., J.L.M., J.W., J.R.M.-M.; Supervision: J.L.M., J.W., J.R.M.-M.; Project administration: J.R.M.-M.; Funding acquisition: J.L.G.-S., J.W., J.R.M.-M.

Funding

The authors' research is supported by the European Molecular Biology Organization, by The Company of Biologists, by Universidad Pablo de Olavide and by the Formación de Personal Investigador-Ministerio de Ciencia e Innovación program (all to J.V.-M.). This work was supported by grants from the Ministerio de Economía, Industria y Competitividad de España (BFU2014-53765-P, BFU2016-81887-REDT, BFU2017-86339-P and MDM-2016-0687 to J.R.M.-M.).

Data availability

The DamID-seq data sets have been deposited in GEO under accession number GSE120531.

Supplementary information

Supplementary information available online at
http://dev.biologists.org/lookup/doi/10.1242/dev.173286.supplemental

References

Agarwala, S., Duquesne, S., Liu, K., Boehm, A., Grimm, L., Link, S., König, S., Eimer, S., Ronneberger, O. and Lecaudey, V. (2015). Amotl2a interacts with the Hippo effector Yap1 and the Wnt/beta-catenin effector Lef1 to control tissue size in zebrafish. *eLife* **4**, e08201. doi:10.7554/eLife.08201

Amores, A., Force, A., Yan, Y. L., Joly, L., Amemiya, C., Fritz, A., Ho, R. K., Langeland, J., Prince, V., Wang, Y. L. et al. (1998). Zebrafish hox clusters and vertebrate genome evolution. *Science* **282**, 1711-1714. doi:10.1126/science.282.5394.1711

Aragona, M., Panciera, T., Manfrin, A., Giulitti, S., Michielin, F., Elvassore, N., Dupont, S. and Piccolo, S. (2013). A mechanical checkpoint controls multicellular growth through YAP/TAZ regulation by actin-processing factors. *Cell* **154**, 1047-1059. doi:10.1016/j.cell.2013.07.042

Aughey, G. N. and Southall, T. D. (2016). Dam it's good! DamID profiling of protein-DNA interactions. *Wiley Interdiscip. Rev. Dev. Biol.* **5**, 25-37. doi:10.1002/wdev.205

Bailey, T. L. (2011). DREME: motif discovery in transcription factor ChIP-seq data. *Bioinformatics* **27**, 1653-1659. doi:10.1093/bioinformatics/btr261

Bandura, J. L. and Edgar, B. A. (2008). Yorkie and Scalloped: partners in growth activation. *Dev. Cell* **14**, 315-316. doi:10.1016/j.devcel.2008.02.010

Betancur, R. R., Wiley, E. O., Arratia, G., Acero, A., Bailly, N., Miya, M., Lecointre, G. and Ortí, G. (2017). Phylogenetic classification of bony fishes. *BMC Evol. Biol.* **17**, 162. doi:10.1186/s12862-017-0958-3

Boc, A., Diallo, A. B. and Makarenkov, V. (2012). T-REX: a web server for inferring, validating and visualizing phylogenetic trees and networks. *Nucleic Acids Res.* **40**, W573-W579. doi:10.1093/nar/gks485

Calvo, F., Ege, N., Grande-Garcia, A., Hooper, S., Jenkins, R. P., Chaudhry, S. I., Harrington, K., Williamson, P., Moeendarbary, E., Charras, G. et al. (2013). Mechanotransduction and YAP-dependent matrix remodelling is required for the generation and maintenance of cancer-associated fibroblasts. *Nat. Cell Biol.* **15**, 637-646. doi:10.1038/ncb2756

Cebola, I., Rodríguez-Seguí, S. A., Cho, C. H.-H., Bessa, J., Rovira, M., Luengo, M., Chhatriwala, M., Berry, A., Ponsa-Cobas, J., Maestro, M. A. et al. (2015). TEAD and YAP regulate the enhancer network of human embryonic pancreatic progenitors. *Nat. Cell Biol.* **17**, 615-626. doi:10.1038/ncb3160

Cheetham, S. W., Gruhn, W. H., van den Ameele, J., Krautz, R., Southall, T. D., Kobayashi, T., Surani, M. A. and Brand, A. H. (2018). Targeted DamID reveals differential binding of mammalian pluripotency factors. *Development* **145**, dev170209. doi:10.1242/dev.170209

Dehal, P. and Boore, J. L. (2005). Two rounds of whole genome duplication in the ancestral vertebrate. *PLoS Biol.* **3**, e314. doi:10.1371/journal.pbio.0030314

Deng, Y., Wu, L. M. N., Bai, S., Zhao, C., Wang, H., Wang, J., Xu, L., Sakabe, M., Zhou, W., Xin, M. et al. (2017). A reciprocal regulatory loop between TAZ/YAP and G-protein Galphas regulates Schwann cell proliferation and myelination. *Nat. Commun.* **8**, 15161. doi:10.1038/ncomms15161

Dupont, S., Morsut, L., Aragona, M., Enzo, E., Giulitti, S., Cordenonsi, M., Zanconato, F., Le Digabel, J., Forcato, M., Bicciato, S. et al. (2011). Role of YAP/TAZ in mechanotransduction. *Nature* **474**, 179-183. doi:10.1038/nature10137

Elbediwy, A. and Thompson, B. J. (2018). Evolution of mechanotransduction via YAP/TAZ in animal epithelia. *Curr. Opin. Cell Biol.* **51**, 117-123. doi:10.1016/j.ceb.2018.02.003

Elosegui-Artola, A., Oria, R., Chen, Y., Kosmalska, A., Pérez-González, C., Castro, N., Zhu, C., Trepat, X. and Roca-Cusachs, P. (2016). Mechanical regulation of a molecular clutch defines force transmission and transduction in response to matrix rigidity. *Nat. Cell Biol.* **18**, 540-548. doi:10.1038/ncb3336

Elosegui-Artola, A., Andreu, I., Beedle, A. E. M., Lezamiz, A., Uroz, M., Kosmalska, A. J., Oria, R., Kechagia, J. Z., Rico-Lastres, P., Le Roux, A. L. et al. (2017). Force triggers YAP nuclear entry by regulating transport across nuclear pores. *Cell* **171**, 1397-1410.e1314. doi:10.1016/j.cell.2017.10.008

Estarás, C., Hsu, H.-T., Huang, L. and Jones, K. A. (2017). YAP repression of the WNT3 gene controls hESC differentiation along the cardiac mesoderm lineage. *Genes Dev.* **31**, 2250-2263. doi:10.1101/gad.307512.117

Galli, G. G., Carrara, M., Yuan, W.-C., Valdes-Quezada, C., Gurung, B., Pepe-Mooney, B., Zhang, T., Geeven, G., Gray, N. S., de Laat, W. et al. (2015). YAP drives growth by controlling transcriptional pause release from dynamic enhancers. *Mol. Cell* **60**, 328-337. doi:10.1016/j.molcel.2015.09.001

Grant, C. E., Bailey, T. L. and Noble, W. S. (2011). FIMO: scanning for occurrences of a given motif. *Bioinformatics* **27**, 1017-1018. doi:10.1093/bioinformatics/btr064

Gutierrez-Triana, J. A., Mateo, J. L., Ibberson, D., Ryu, S. and Wittbrodt, J. (2016). iDamIDseq and iDEAR: an improved method and computational pipeline to profile chromatin-binding proteins. *Development* **143**, 4272-4278. doi:10.1242/dev.139261

Harvey, K. F., Pfleger, C. M. and Hariharan, I. K. (2003). The Drosophila Mst ortholog, hippo, restricts growth and cell proliferation and promotes apoptosis. *Cell* **114**, 457-467. doi:10.1016/S0092-8674(03)00557-9

Hilman, D. and Gat, U. (2011). The evolutionary history of YAP and the hippo/YAP pathway. *Mol. Biol. Evol.* **28**, 2403-2417. doi:10.1093/molbev/msr065

Huang, J., Wu, S., Barrera, J., Matthews, K. and Pan, D. (2005). The Hippo signaling pathway coordinately regulates cell proliferation and apoptosis by inactivating Yorkie, the Drosophila Homolog of YAP. *Cell* **122**, 421-434. doi:10.1016/j.cell.2005.06.007

Iwamatsu, T. (2004). Stages of normal development in the medaka Oryzias latipes. *Mech. Dev.* **121**, 605-618. doi:10.1016/j.mod.2004.03.012

Kanai, F., Marignani, P. A., Sarbassova, D., Yagi, R., Hall, R. A., Donowitz, M., Hisaminato, A., Fujiwara, T., Ito, Y., Cantley, L. C. et al. (2000). TAZ: a novel transcriptional co-activator regulated by interactions with 14-3-3 and PDZ domain proteins. *EMBO J.* **19**, 6778-6791. doi:10.1093/emboj/19.24.6778

Kimelman, D., Smith, N. L., Lai, J. K. H. and Stainier, D. Y. R. (2017). Regulation of posterior body and epidermal morphogenesis in zebrafish by localized Yap1 and Wwtr1. *eLife* **6**, e31065. doi:10.7554/eLife.31065

Kimmel, C. B., Ballard, W. W., Kimmel, S. R., Ullmann, B. and Schilling, T. F. (1995). Stages of embryonic development of the zebrafish. *Dev. Dyn.* **203**, 253-310. doi:10.1002/aja.1002030302

Lee, D.-H., Park, J. O., Kim, T.-S., Kim, S.-K., Kim, T.-H., Kim, M.-C., Park, G. S., Kim, J.-H., Kuninaka, S., Olson, E. N. et al. (2016). LATS-YAP/TAZ controls lineage specification by regulating TGFbeta signaling and Hnf4alpha expression during liver development. *Nat. Commun.* **7**, 11961. doi:10.1038/ncomms11961

Levy, D., Adamovich, Y., Reuven, N. and Shaul, Y. (2008). Yap1 phosphorylation by c-Abl is a critical step in selective activation of proapoptotic genes in response to DNA damage. *Mol. Cell* **29**, 350-361. doi:10.1016/j.molcel.2007.12.022

Li, Z., Zhao, B., Wang, P., Chen, F., Dong, Z., Yang, H., Guan, K.-L. and Xu, Y. (2010). Structural insights into the YAP and TEAD complex. *Genes Dev.* **24**, 235-240. doi:10.1101/gad.1865810

Li, P., Silvis, M. R., Honaker, Y., Lien, W.-H., Arron, S. T. and Vasioukhin, V. (2016). alphaE-catenin inhibits a Src-YAP1 oncogenic module that couples tyrosine kinases and the effector of Hippo signaling pathway. *Genes Dev.* **30**, 798-811. doi:10.1101/gad.274951.115

Lian, I., Kim, J., Okazawa, H., Zhao, J., Zhao, B., Yu, J., Chinnaiyan, A., Israel, M. A., Goldstein, L. S. B., Abujarour, R. et al. (2010). The role of YAP transcription coactivator in regulating stem cell self-renewal and differentiation. *Genes Dev.* **24**, 1106-1118. doi:10.1101/gad.1903310

Lin, C., Yao, E., Zhang, K., Jiang, X., Croll, S., Thompson-Peer, K. and Chuang, P. T. (2017). YAP is essential for mechanical force production and epithelial cell proliferation during lung branching morphogenesis. *eLife* **6**, e21130. doi:10.7554/eLife.21130

Marlétaz, F., Firbas, P. N., Maeso, I., Tena, J. J., Bogdanovic, O., Perry, M., Wyatt, C. D. R., de la Calle-Mustienes, E., Bertrand, S., Burguera, D. et al. (2018). Amphioxus functional genomics and the origins of vertebrate gene regulation. *Nature* **564**, 64-70. doi:10.1038/s41586-018-0734-6

Marshall, O. J. and Brand, A. H. (2017). Chromatin state changes during neural development revealed by in vivo cell-type specific profiling. *Nat. Commun.* **8**, 2271. doi:10.1038/s41467-017-02385-4

Marshall, O. J., Southall, T. D., Cheetham, S. W. and Brand, A. H. (2016). Cell-type-specific profiling of protein-DNA interactions without cell isolation using targeted DamID with next-generation sequencing. *Nat. Protoc.* **11**, 1586-1598. doi:10.1038/nprot.2016.084

McLeay, R. C. and Bailey, T. L. (2010). Motif Enrichment Analysis: a unified framework and an evaluation on ChIP data. *BMC Bioinformatics* **11**, 165. doi:10.1186/1471-2105-11-165

Meng, Z., Moroishi, T. and Guan, K.-L. (2016). Mechanisms of Hippo pathway regulation. *Genes Dev.* **30**, 1-17. doi:10.1101/gad.274027.115

Mi, H., Muruganujan, A. and Thomas, P. D. (2013). PANTHER in 2013: modeling the evolution of gene function, and other gene attributes, in the context of phylogenetic trees. *Nucleic Acids Res.* **41**, D377-D386. doi:10.1093/nar/gks1118

Mi, H., Huang, X., Muruganujan, A., Tang, H., Mills, C., Kang, D. and Thomas, P. D. (2017). PANTHER version 11: expanded annotation data from Gene Ontology and Reactome pathways, and data analysis tool enhancements. *Nucleic Acids Res.* **45**, D183-D189. doi:10.1093/nar/gkw1138

Miesfeld, J. B., Gestri, G., Clark, B. S., Flinn, M. A., Poole, R. J., Bader, J. R., Besharse, J. C., Wilson, S. W. and Link, B. A. (2015). Yap and Taz regulate retinal pigment epithelial cell fate. *Development* **142**, 3021-3032. doi:10.1242/dev.119008

Moreno-Mateos, M. A., Vejnar, C. E., Beaudoin, J.-D., Fernandez, J. P., Mis, E. K., Khokha, M. K. and Giraldez, A. J. (2015). CRISPRscan: designing highly efficient sgRNAs for CRISPR-Cas9 targeting in vivo. *Nat. Methods* **12**, 982-988. doi:10.1038/nmeth.3543

Morin-Kensicki, E. M., Boone, B. N., Howell, M., Stonebraker, J. R., Teed, J., Alb, J. G., Magnuson, T. R., O'Neal, W. and Milgram, S. L. (2006). Defects in yolk sac vasculogenesis, chorioallantoic fusion, and embryonic axis elongation in mice with targeted disruption of Yap65. *Mol. Cell. Biol.* **26**, 77-87. doi:10.1128/MCB.26.1.77-87.2006

Nardone, G., Oliver-De La Cruz, J., Vrbsky, J., Martini, C., Pribyl, J., Skládal, P., Pešl, M., Caluori, G., Pagliari, S., Martino, F. et al. (2017). YAP regulates cell mechanics by controlling focal adhesion assembly. *Nat. Commun.* **8**, 15321. doi:10.1038/ncomms15321

Nishioka, N., Inoue, K., Adachi, K., Kiyonari, H., Ota, M., Ralston, A., Yabuta, N., Hirahara, S., Stephenson, R. O., Ogonuki, N. et al. (2009). The Hippo signaling pathway components Lats and Yap pattern Tead4 activity to distinguish mouse trophectoderm from inner cell mass. *Dev. Cell* **16**, 398-410. doi:10.1016/j.devcel.2009.02.003

Piccolo, S., Dupont, S. and Cordenonsi, M. (2014). The biology of YAP/TAZ: hippo signaling and beyond. *Physiol. Rev.* **94**, 1287-1312. doi:10.1152/physrev.00005.2014

Pinheiro, L. B., Coleman, V. A., Hindson, C. M., Herrmann, J., Hindson, B. J., Bhat, S. and Emslie, K. R. (2012). Evaluation of a droplet digital polymerase chain reaction format for DNA copy number quantification. *Anal. Chem.* **84**, 1003-1011. doi:10.1021/ac202578x

Porazinski, S., Wang, H., Asaoka, Y., Behrndt, M., Miyamoto, T., Morita, H., Hata, S., Sasaki, T., Krens, S. F. G., Osada, Y. et al. (2015). YAP is essential for tissue tension to ensure vertebrate 3D body shape. *Nature* **521**, 217-221. doi:10.1038/nature14215

Rosenbluh, J., Nijhawan, D., Cox, A. G., Li, X., Neal, J. T., Schafer, E. J., Zack, T. I., Wang, X., Tsherniak, A., Schinzel, A. C. et al. (2012). beta-Catenin-driven cancers require a YAP1 transcriptional complex for survival and tumorigenesis. *Cell* **151**, 1457-1473. doi:10.1016/j.cell.2012.11.026

Shannon, P., Markiel, A., Ozier, O., Baliga, N. S., Wang, J. T., Ramage, D., Amin, N., Schwikowski, B. and Ideker, T. (2003). Cytoscape: a software environment for integrated models of biomolecular interaction networks. *Genome Res.* **13**, 2498-2504. doi:10.1101/gr.1239303

Singh, A., Ramesh, S., Cibi, D. M., Yun, L. S., Li, J., Li, L., Manderfield, L. J., Olson, E. N., Epstein, J. A. and Singh, M. K. (2016). Hippo signaling mediators Yap and Taz are required in the epicardium for coronary vasculature development. *Cell Rep.* **15**, 1384-1393. doi:10.1016/j.celrep.2016.04.027

Southall, T. D., Gold, K. S., Egger, B., Davidson, C. M., Caygill, E. E., Marshall, O. J. and Brand, A. H. (2013). Cell-type-specific profiling of gene expression and chromatin binding without cell isolation: assaying RNA Pol II occupancy in neural stem cells. *Dev. Cell* **26**, 101-112. doi:10.1016/j.devcel.2013.05.020

Stein, C., Bardet, A. F., Roma, G., Bergling, S., Clay, I., Ruchti, A., Agarinis, C., Schmelzle, T., Bouwmeester, T., Schübeler, D. et al. (2015). YAP1 exerts its transcriptional control via TEAD-mediated activation of enhancers. *PLoS Genet.* **11**, e1005465. doi:10.1371/journal.pgen.1005465

Stemmer, M., Thumberger, T., Del Sol Keyer, M., Wittbrodt, J. and Mateo, J. L. (2015). CCTop: an intuitive, flexible and reliable CRISPR/Cas9 target prediction tool. *PLoS ONE* **10**, e0124633. doi:10.1371/journal.pone.0124633

Sudol, M. (1994). Yes-associated protein (YAP65) is a proline-rich phosphoprotein that binds to the SH3 domain of the Yes proto-oncogene product. *Oncogene* **9**, 2145-2152.

Tamm, C., Bower, N. and Anneren, C. (2011). Regulation of mouse embryonic stem cell self-renewal by a Yes-YAP-TEAD2 signaling pathway downstream of LIF. *J. Cell Sci.* **124**, 1136-1144. doi:10.1242/jcs.075796

Taniguchi, K., Wu, L.-W., Grivennikov, S. I., de Jong, P. R., Lian, I., Yu, F.-X., Wang, K., Ho, S. B., Boland, B. S., Chang, J. T. et al. (2015). A gp130-Src-YAP module links inflammation to epithelial regeneration. *Nature* **519**, 57-62. doi:10.1038/nature14228

Tapon, N., Harvey, K. F., Bell, D. W., Wahrer, D. C. R., Schiripo, T. A., Haber, D. A. and Hariharan, I. K. (2002). salvador Promotes both cell cycle exit and apoptosis in Drosophila and is mutated in human cancer cell lines. *Cell* **110**, 467-478. doi:10.1016/S0092-8674(02)00824-3

Thisse, C. and Thisse, B. (2008). High-resolution in situ hybridization to whole-mount zebrafish embryos. *Nat. Protoc.* **3**, 59-69. doi:10.1038/nprot.2007.514

Thisse, B., Pflumio, S., Fürthauer, M., Loppin, B., Heyer, V., Degrave, A., Woehl, R., Lux, A., Steffan, T., Charbonnier, X. Q. et al. (2001). Expression of the zebrafish genome during embryogenesis. In ZFIN Direct Data Submission (https://zfin.org/ZDB-PUB-010810-1).

Tosti, L., Ashmore, J., Tan, B. S. N., Carbone, B., Mistri, T. K., Wilson, V., Tomlinson, S. R. and Kaji, K. (2018). Mapping transcription factor occupancy using minimal numbers of cells in vitro and in vivo. *Genome Res.* **28**, 592-605. doi:10.1101/gr.227124.117

van Steensel, B., Delrow, J. and Henikoff, S. (2001). Chromatin profiling using targeted DNA adenine methyltransferase. *Nat. Genet.* **27**, 304-308. doi:10.1038/85871

Varelas, X. (2014). The Hippo pathway effectors TAZ and YAP in development, homeostasis and disease. *Development* **141**, 1614-1626. doi:10.1242/dev.102376

Vassilev, A., Kaneko, K. J., Shu, H., Zhao, Y. and DePamphilis, M. L. (2001). TEAD/TEF transcription factors utilize the activation domain of YAP65, a Src/Yes-associated protein localized in the cytoplasm. *Genes Dev.* **15**, 1229-1241. doi:10.1101/gad.888601

Vlahov, N., Scrace, S., Soto, M. S., Grawenda, A. M., Bradley, L., Pankova, D., Papaspyropoulos, A., Yee, K. S., Buffa, F., Goding, C. R. et al. (2015). Alternate RASSF1 transcripts control SRC activity, E-cadherin contacts, and YAP-mediated invasion. *Curr. Biol.* **25**, 3019-3034. doi:10.1016/j.cub.2015.09.072

Webb, C., Upadhyay, A., Giuntini, F., Eggleston, I., Furutani-Seiki, M., Ishima, R. and Bagby, S. (2011). Structural features and ligand binding properties of tandem WW domains from YAP and TAZ, nuclear effectors of the Hippo pathway. *Biochemistry* **50**, 3300-3309. doi:10.1021/bi2001888

Wu, S., Huang, J., Dong, J. and Pan, D. (2003). hippo encodes a Ste-20 family protein kinase that restricts cell proliferation and promotes apoptosis in conjunction with salvador and warts. *Cell* **114**, 445-456. doi:10.1016/S0092-8674(03)00549-X

Xin, M., Kim, Y., Sutherland, L. B., Murakami, M., Qi, X., McAnally, J., Porrello, E. R., Mahmoud, A. I., Tan, W., Shelton, J. M. et al. (2013). Hippo pathway effector Yap promotes cardiac regeneration. *Proc. Natl. Acad. Sci. USA* **110**, 13839-13844. doi:10.1073/pnas.1313192110

Yu, C., Ji, S.-Y., Dang, Y.-J., Sha, Q.-Q., Yuan, Y.-F., Zhou, J.-J., Yan, L.-Y., Qiao, J., Tang, F. and Fan, H.-Y. (2016). Oocyte-expressed yes-associated protein is a key activator of the early zygotic genome in mouse. *Cell Res.* **26**, 275-287. doi:10.1038/cr.2016.20

Zaidi, S. K., Sullivan, A. J., Medina, R., Ito, Y., van Wijnen, A. J., Stein, J. L., Lian, J. B. and Stein, G. S. (2004). Tyrosine phosphorylation controls Runx2-mediated subnuclear targeting of YAP to repress transcription. *EMBO J.* **23**, 790-799. doi:10.1038/sj.emboj.7600073

Zanconato, F., Forcato, M., Battilana, G., Azzolin, L., Quaranta, E., Bodega, B., Rosato, A., Bicciato, S., Cordenonsi, M. and Piccolo, S. (2015). Genome-wide association between YAP/TAZ/TEAD and AP-1 at enhancers drives oncogenic growth. *Nat. Cell Biol.* **17**, 1218-1227. doi:10.1038/ncb3216

Zanconato, F., Cordenonsi, M. and Piccolo, S. (2016). YAP/TAZ at the roots of cancer. *Cancer Cell* **29**, 783-803. doi:10.1016/j.ccell.2016.05.005

Zhang, L., Ren, F., Zhang, Q., Chen, Y., Wang, B. and Jiang, J. (2008). The TEAD/TEF family of transcription factor Scalloped mediates Hippo signaling in organ size control. *Dev. Cell* **14**, 377-387. doi:10.1016/j.devcel.2008.01.006

Zhao, B., Ye, X., Yu, J., Li, L., Li, W., Li, S., Yu, J., Lin, J. D., Wang, C.-Y., Chinnaiyan, A. M. et al. (2008). TEAD mediates YAP-dependent gene induction and growth control. *Genes Dev.* **22**, 1962-1971. doi:10.1101/gad.1664408

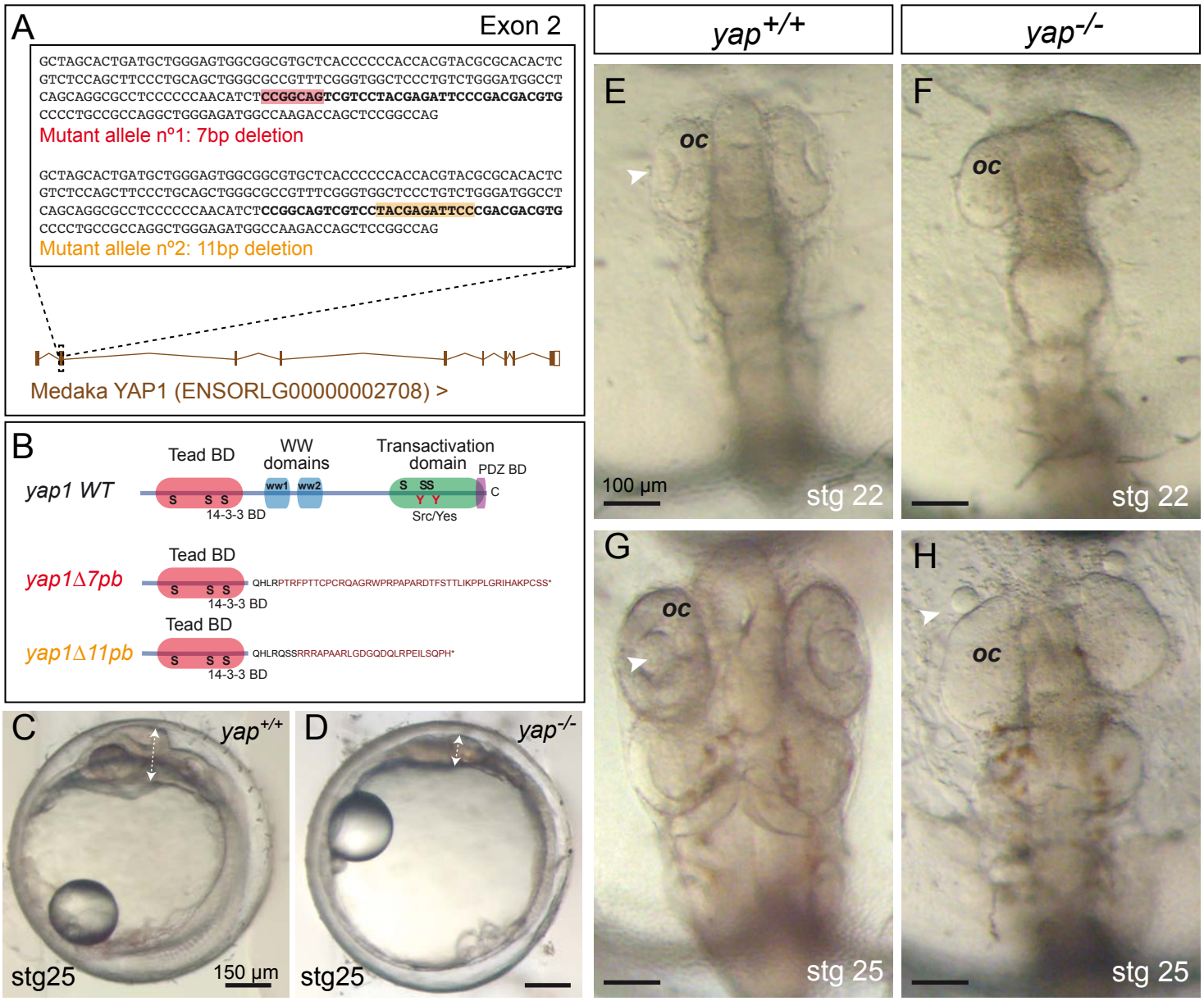

Figure S1: Generation of *yap1* mutant alleles by CRISPR/Cas9 genome editing. (A) Schematic representation of the 7 bp and 11 bp deletions generated in the exon 2 of *yap1* in medaka. The sequence in bold corresponds to the region targeted by two partially overlapping sgRNAs (see Methods). The boxes in red and orange correspond to the 7 and 11 bp deletions generated. (B) The predicted yap1 protein structure is depicted for the wild type and mutant proteins. In both cases, the deletions resulted in frame shift mutations and premature stop codons. (C-H) Phenotypic analysis of wild type (C, E, G) and *yap1* mutant embryos (D, F, H) at stages 22 (E-F) and 25 (C-D, G-H) shows characteristic malformations, such as optic cup flattening and lens misalignment (arrows in H). oc = optic cup. Magnification bars are included in the figure.

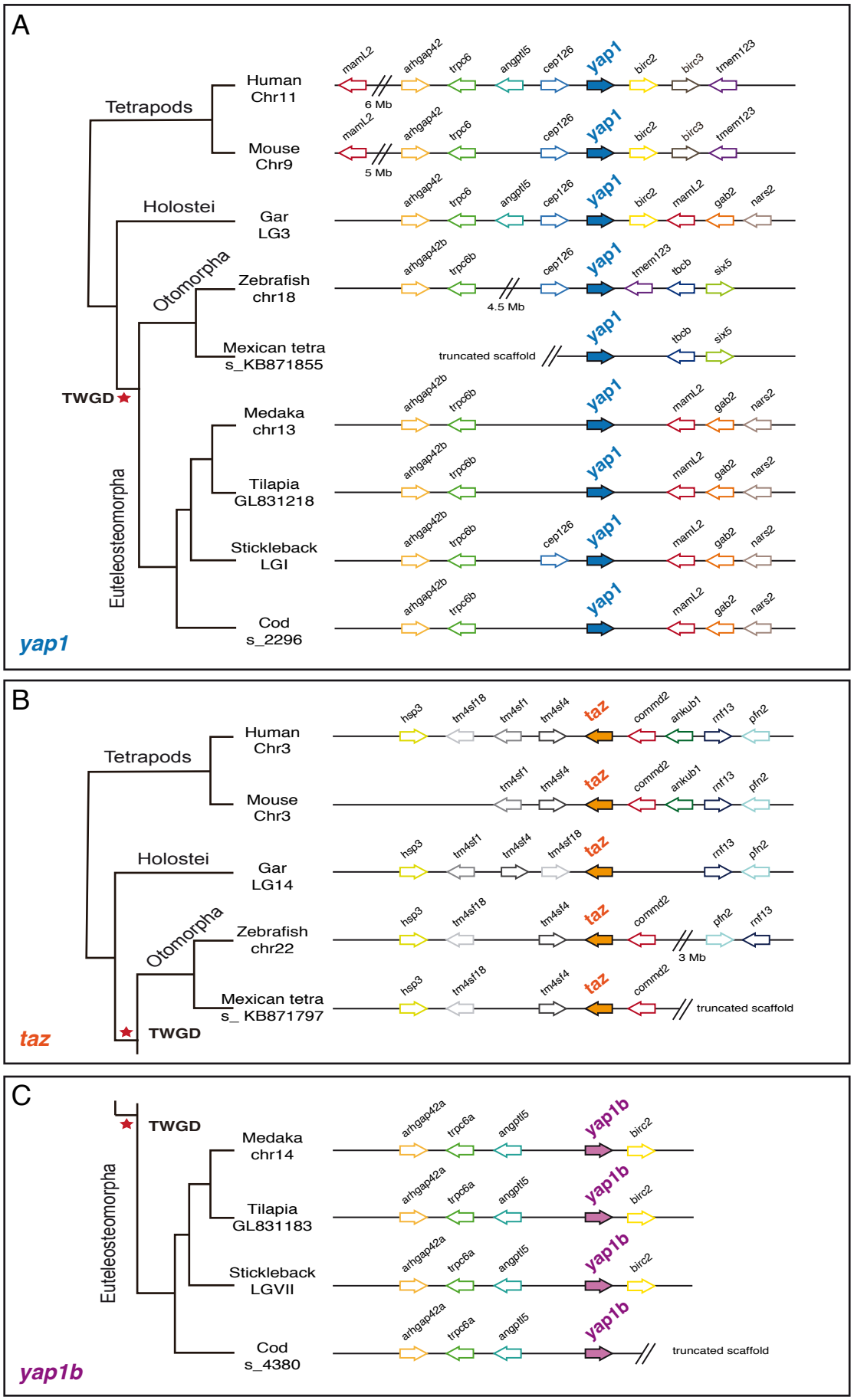

Figure S2: Micro-synteny arrangement around yap family paralogs. (A) Phylogenetic tree displaying gene arrangement around *yap1* for the representative 7 teleost and two tetrapod species analyzed in Figure 1. Note the conserved linkage between *yap1* and the *arhgap42*/*trpc6* block. (B) Phylogenetic tree and gene arrangement around *taz* in different vertebrate branches. Note the conserved linkage between *hsp3*, *taz*, and *commd2*. (C) Linkage of *arhgap42a* and *trpc6a* to *yap1b* shows that this gene emerged by duplication of and ancestral *yap1*. Color-coded arrows indicate both gene orientation and equivalent orthologs in different species. Chromosomes or gene scaffolds are also indicated. TWGD= teleost-specific genome duplication.

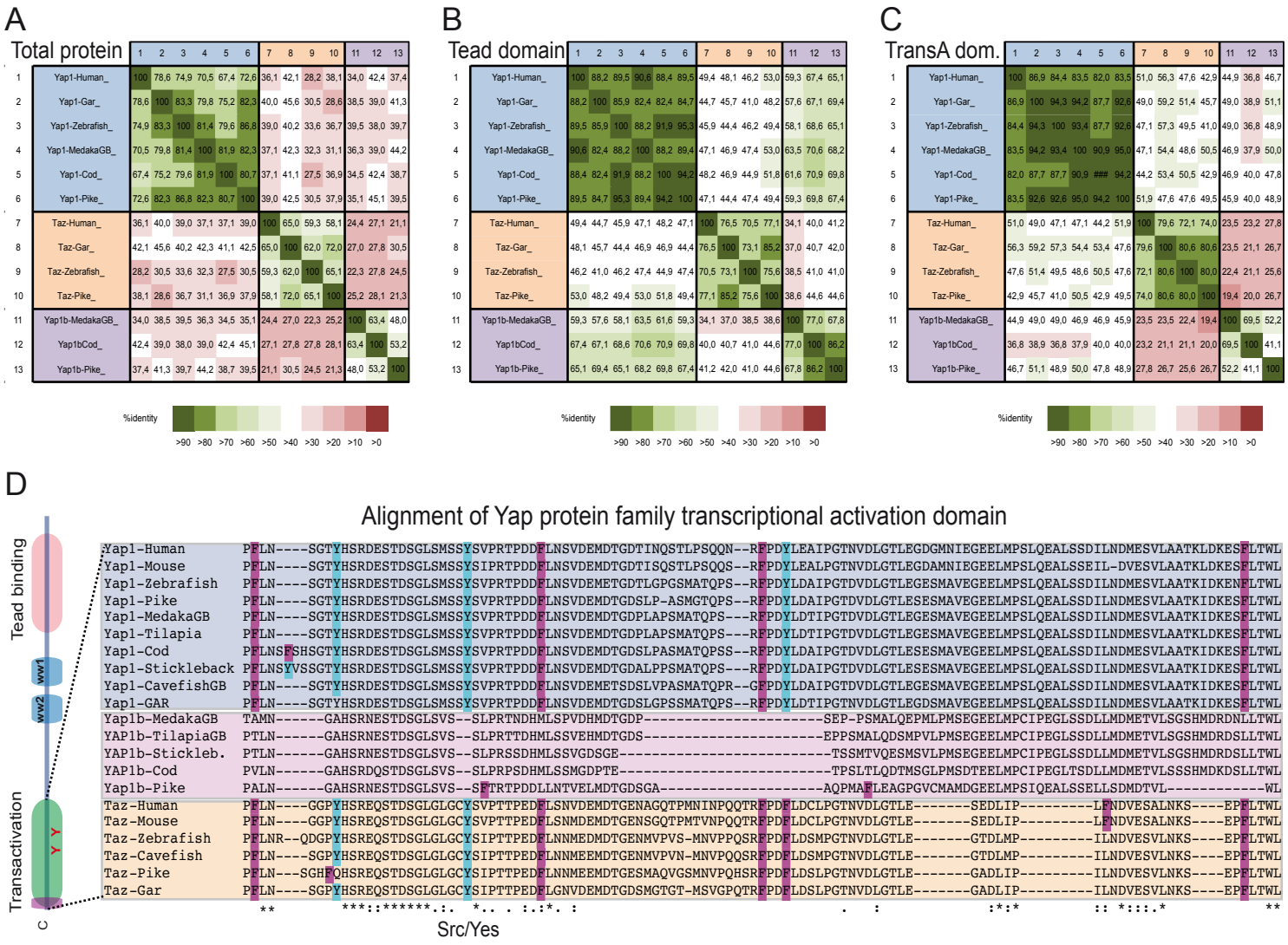

Figure S3: Yap1b Divergent transcriptional activation domain. Heat map representations of sequence homology (aa Identity in %) between Yap family proteins from different species are shown for: (A) the entire protein, (B) TEAD binding domains, and (C) transcriptional activation domains. Note that whereas the Tead binding domain of Yap1b is relatively well conserved with respect to the equivalent domain in Yap1, the transcriptional activation domain shows lower amino acid identity (average aa Identity 65.5 % vs. 44.8 %, respectively). (D) Multiple sequence alignment of the entire transactivation domain of Yap family proteins from different species. Note the elimination or substitution of conserved tyrosine (Blue) and phenylalanine (red) residues in Yap1b proteins. The main tyrosine phosphorylated by Scr-family kinases is indicated.

A

Alignment of Yap family transactivation domain (exon 7)

```
                                                Src/Yes
Taza_AnJa       -GPFHSREQSTDSGLGLGCYSIPTTPEDFLNNVDEMD
Taz_Gar         -GPYHSREQSTDSGLGLGCYSIPTTPEDFLGNVDEMD
Taz_Zebraf      -GPYHSREQSTDSGLGLGCYSIPTTPEDFLNNMEDMD
Taz_Pike        GHFQHSREQSTDSGLGLGCYSIPTTPEDFLNNMEEMD
Tazb_AnJa       -GPYHSREQSTDSGLGLGCYSIPTTPEDILNNVEEMD
Taza_PaKi       -GPYHSREQSTDSGLGLGCYSVPTTPEDFLNNLEEMD
Tazb_PaKi       -GHYHSRDKSTDSGLGLGCCSHPTTPEGFLS-MDEMD
Yap1_AnJa       -GTYHSRDESTDSGLSMSSYSVPRTPDDFLNSVDEMD
Yap1_PaKi       -GTYHSRDESTDSGLSMSSYSVPRTPDDFLNSVDEMD
Yap1_Gar        -GTYHSRDESTDSGLSMSSYSVPRTPDDFLNSVDEMD
Yap1_Tilapia    -GTYHSRDESTDSGLSMSSYSVPRTPDDFLNSVDEMD
Yap1_Pike       -GTYHSRDESTDSGLSMSSYSVPRTPDDFLNSVDEMD
Yap1_Medaka     -GTYHSRDESTDSGLSMSSYSVPRTPDDFLNSVDEMD
Yap1_Zebraf     -GTYHSRDESTDSGLSMSSYSVPRTPDDFLNSVDEME
Yap1b_PaKi      -GTYHSRDESTDSGLSVSSYSVPRTPDDLLNSVEEME
Yap1b_AnJa      -GNFHSRDESTDSGLSVSSYSIPRTPDDFLNSVDEMD
Yap1b_Medaka    -NGAHSRNESTDSGLSVS--SLPRTNDHMLSPVDHMD
Yap1b_Tilapia   -NGAHSRNESTDSGLSVS--SLPRTTDHMLSSVEHMD
Yap1b_Pike      -NGAHSRNESTDSGLSVS--SFTRTPDDLLNTVELMD
                ***::*******.:.  * . * : :*. :: *:
```

B

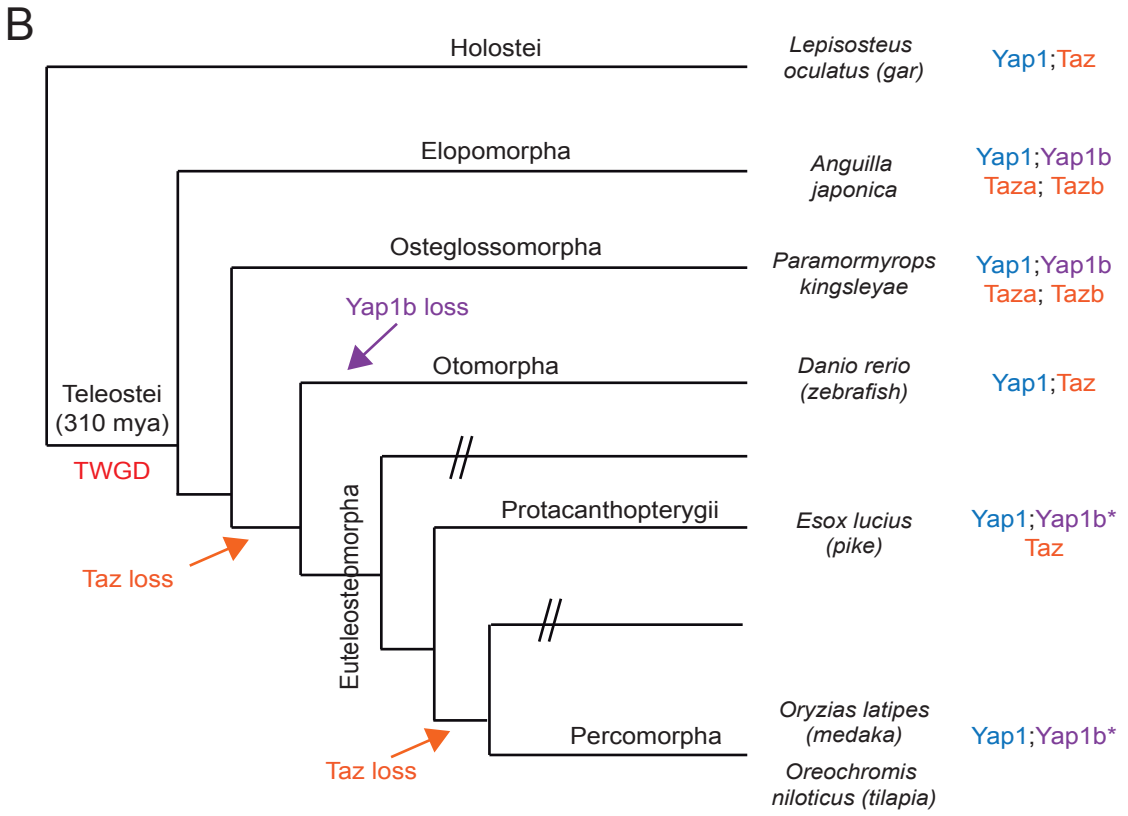

Figure S4: Evolutionary history of Yap family in teleost. (A) Multiple sequence alignment of the N-terminal segment of the transactivation domain in different teleost species. Note that the elimination/substitution, in Yap1b proteins of conserved tyrosine (red) and phenylalanine (light blue) residues occurs in Euteleosteomorpha, but not in Elopomorpha or Osteoglossomorpha species. The main tyrosine residue that can be phosphorylated by Src-family kinases is also indicated. (B) Phylogenetic tree showing the main teleost branches and their evolutionary relationship. The position of the different species considered for the sequence alignment, the different paralogs (color-coded) present in each species, and the evolutionary gene losses are indicated. TWGD= teleost-specific genome duplication.

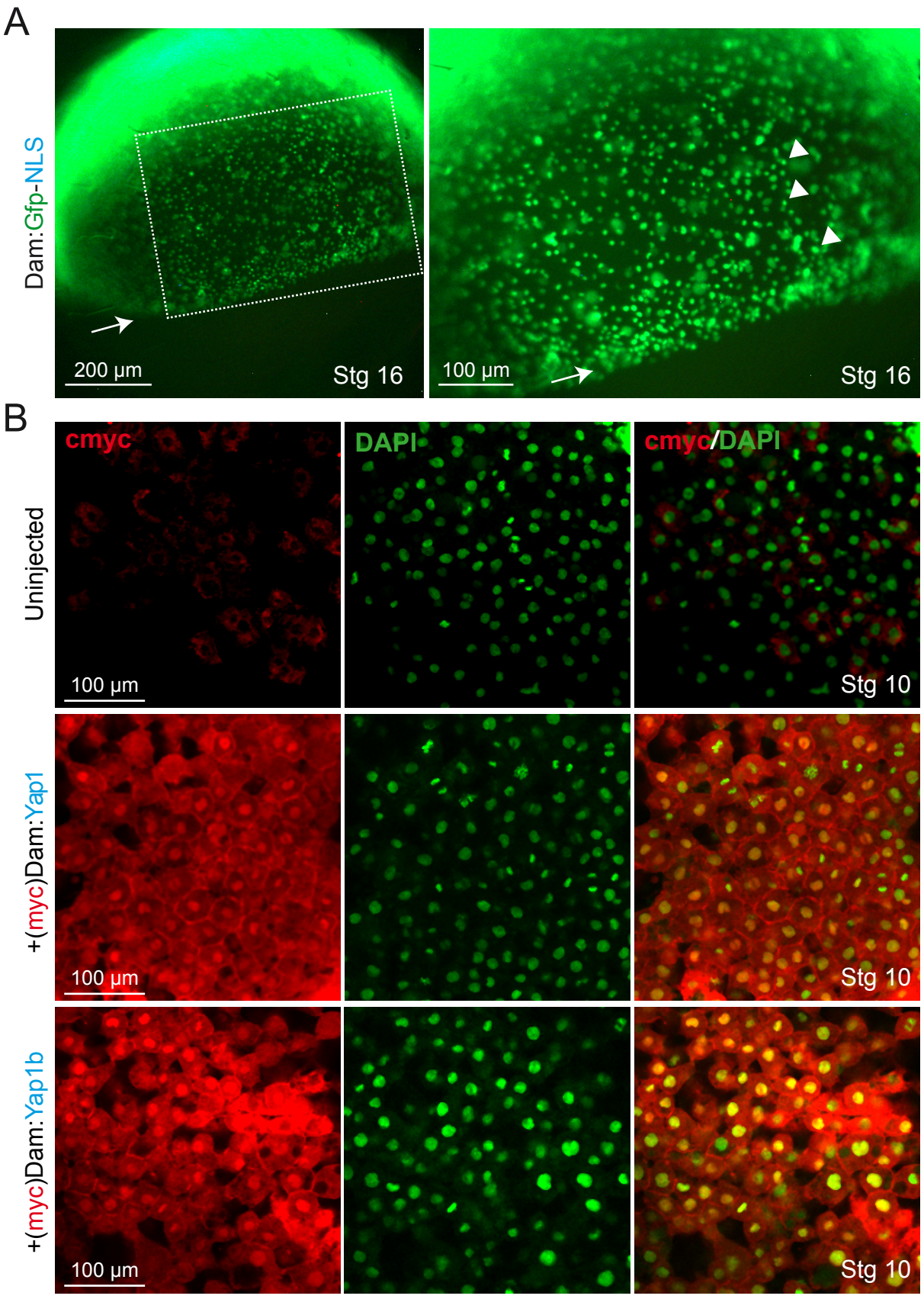

Figure S5: Nuclear localization of DamID fusions. After injection into one-cell stage medaka embryos, the nuclear localization of the DamID fusion proteins was evaluated (A) Fluorescent stereo-microscope images show DAM:GFP-NLS signal at the nuclei (arrowheads) in stage 16 embryos. The epiboly front is indicated (white arrow) (B) Confocal images show the nuclear localization of Dam:Yap1 and Dam:Yap1b, as revealed by immunostaining using anti-myc antibodies in stage 10 embryos. Un-injected embryos were included as a control, and samples were counterstained with DAPI to reveal nuclei position. Bar= 100 µm.

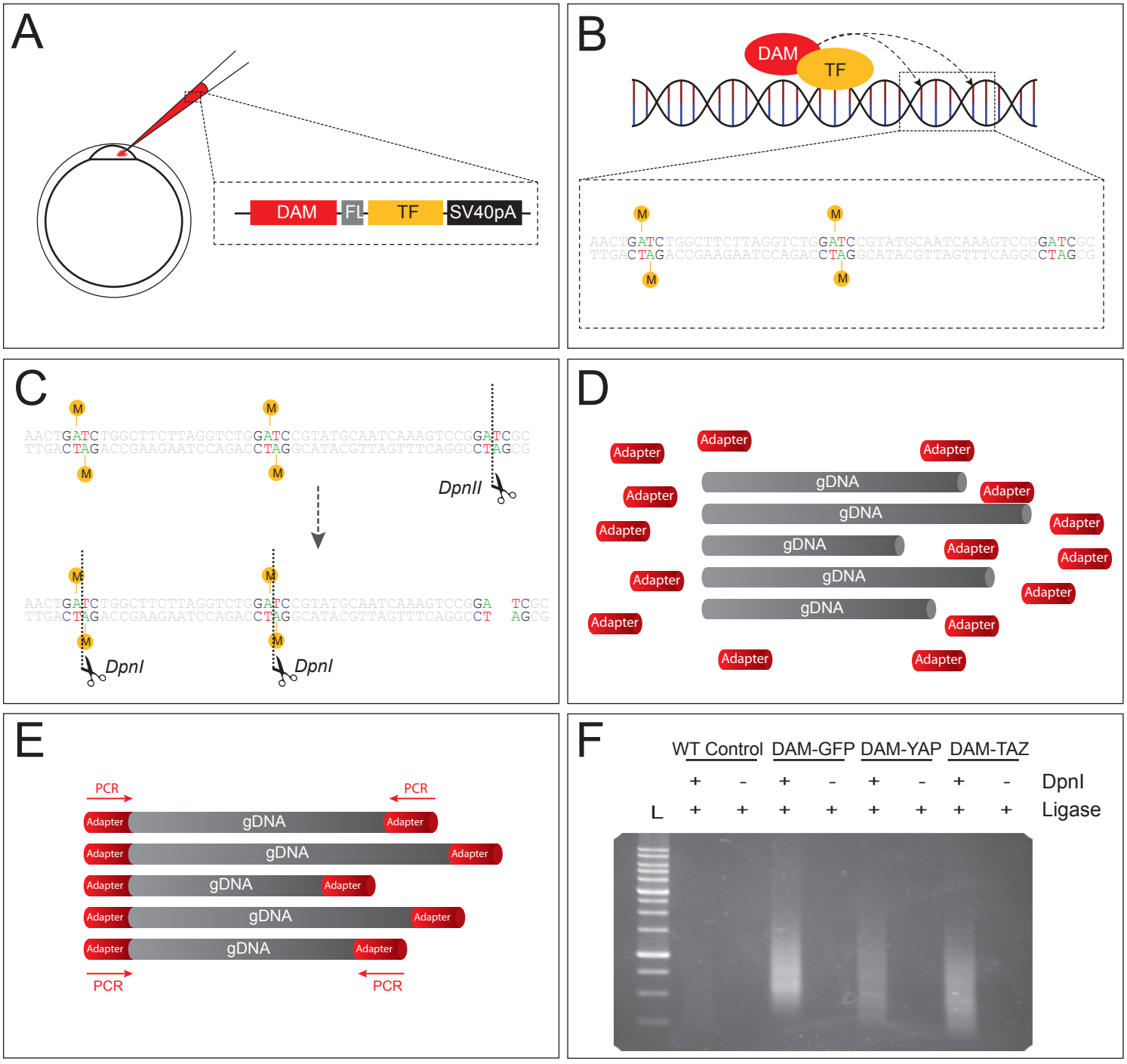

Figure S6: Outline of the DamID-seq protocol. (A) mRNA from the different Dam-TF fusions were injected into medaka or zebrafish embryos at single cell stage. (B) Upon binding of the TF to its transcriptional targets, the DAM protein methylates the adjacent GATC sites. (C) After extracting the gDNA fraction from the injected embryos, the genome is fragmented with DpnII and the methylated GATC sites are further cut using DpnI. (D) Adapters are incorporated at both ends of the resulting fragments. (E) Fragments are amplified using the adapters' sequence to generate the corresponding libraries. (F) Resulting libraries are then visualized as DNA smears on an electrophoresis gel.

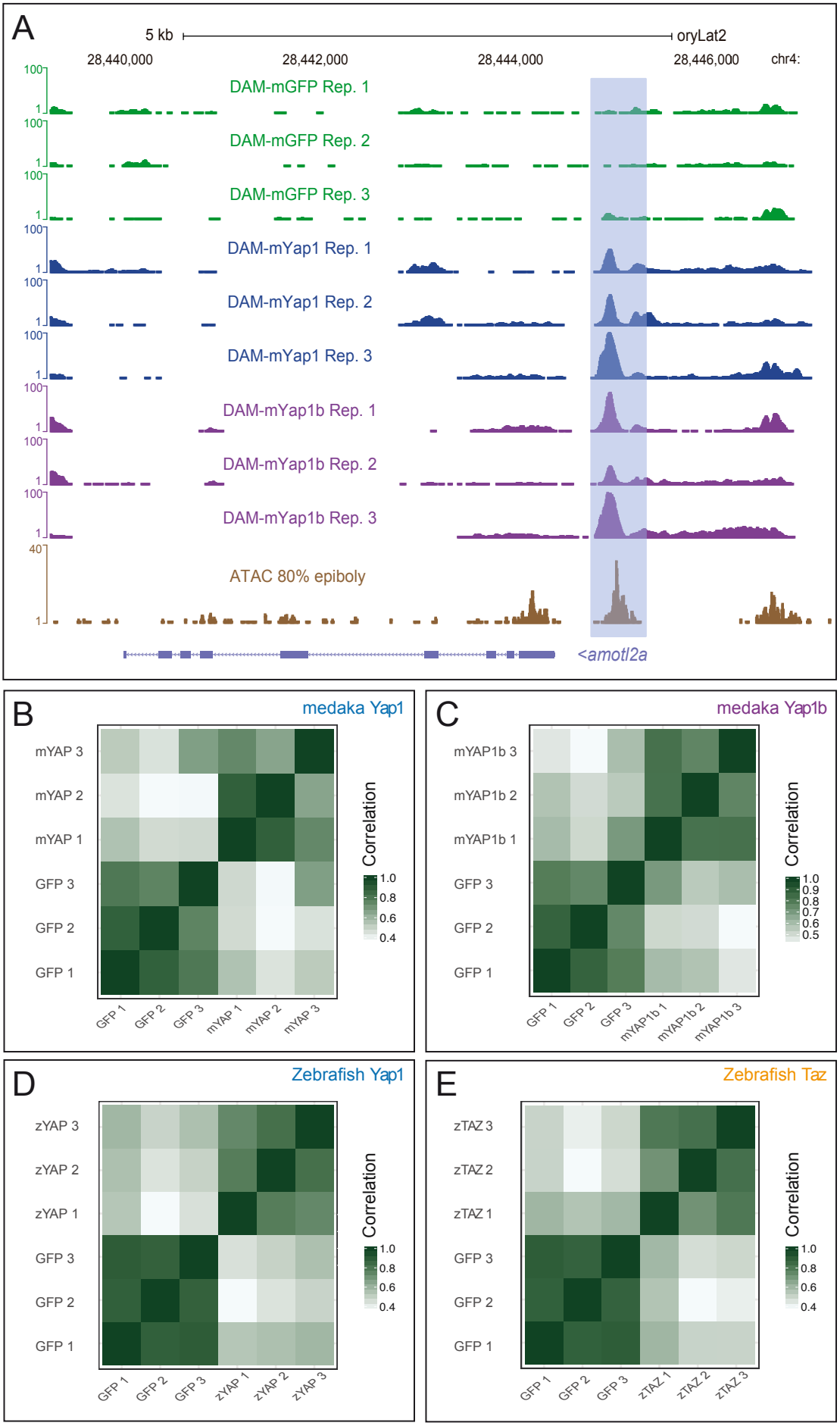

Figure S7: Correlation between DamID-seq experiments. (A) DamID-seq tracks for three independent replicates are shown in the locus of *amotl2a*. Dam-yap1, Dam-yap1b and Dam-GFP peaks, generated from 80% epiboly medaka embryos, are shown in relation to available ATAC-seq marks (see also figure 3). (B-E) Heatmap matrixes showing the correlation coefficient between mapped reads for each of the samples: medaka DAM:yap1 (B), medaka DAM:yap1b (C), zebrafish DAM:yap1 (D), and zebrafish DAM:taz (E), with its replicates (n=3) and its corresponding DAM:GFP controls.

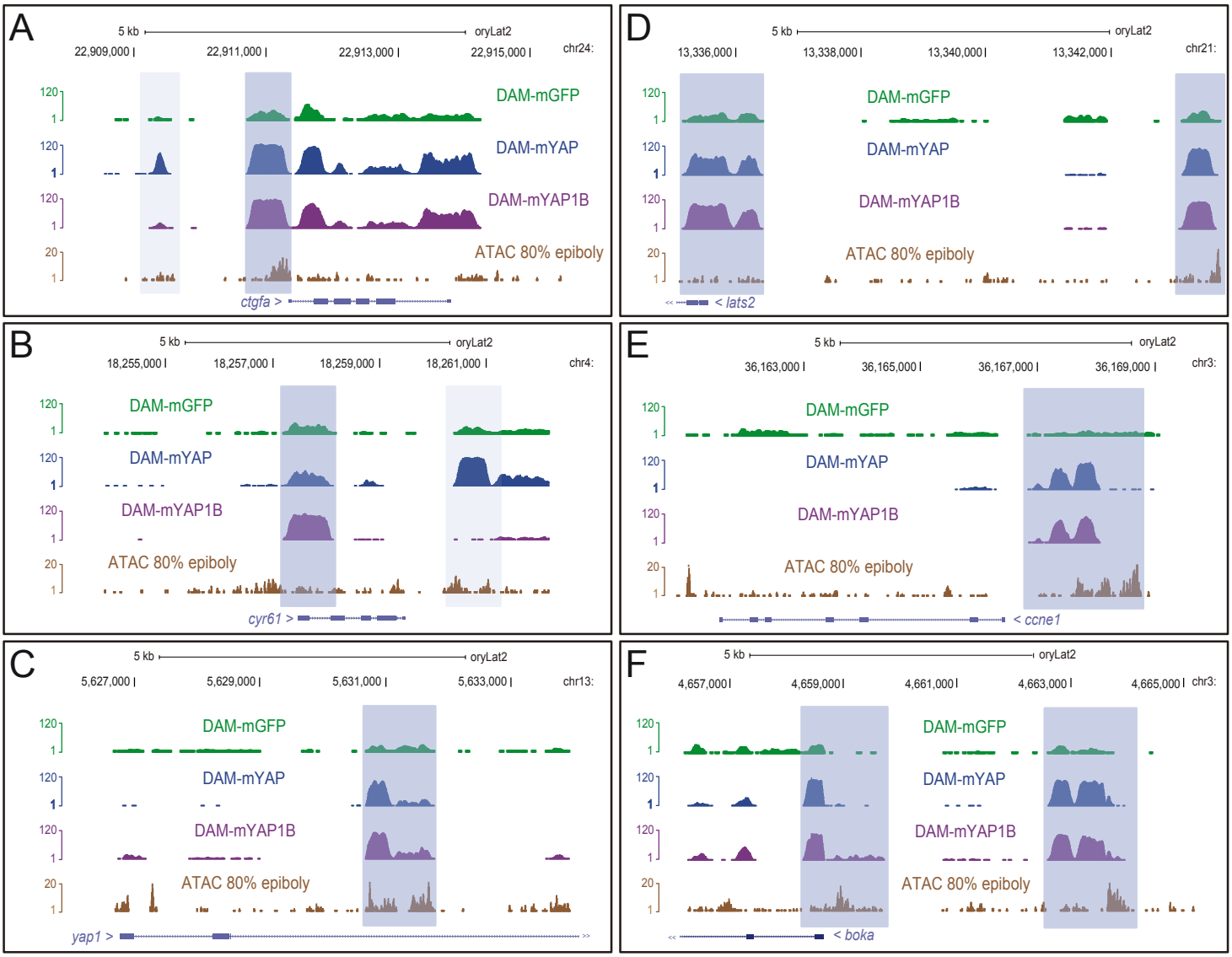

Figure S8: DamID-seq profiling of Yap1 and Yap1b in medaka. Dam-yap1, Dam-yap1b and Dam-GFP tracks from 80% epiboly medaka embryos are shown for several loci harboring known Yap target genes such as: *ctgfa* (A), *cyr61* (B), *yap1* (C), *lats2* (D), *ccne1* (E), and *boka* (F). Peaks are shown in relation to available ATAC-seq marks. Some of the differentially methylated peaks in enhancers, promoters, and introns are highlighted by shadow boxes.

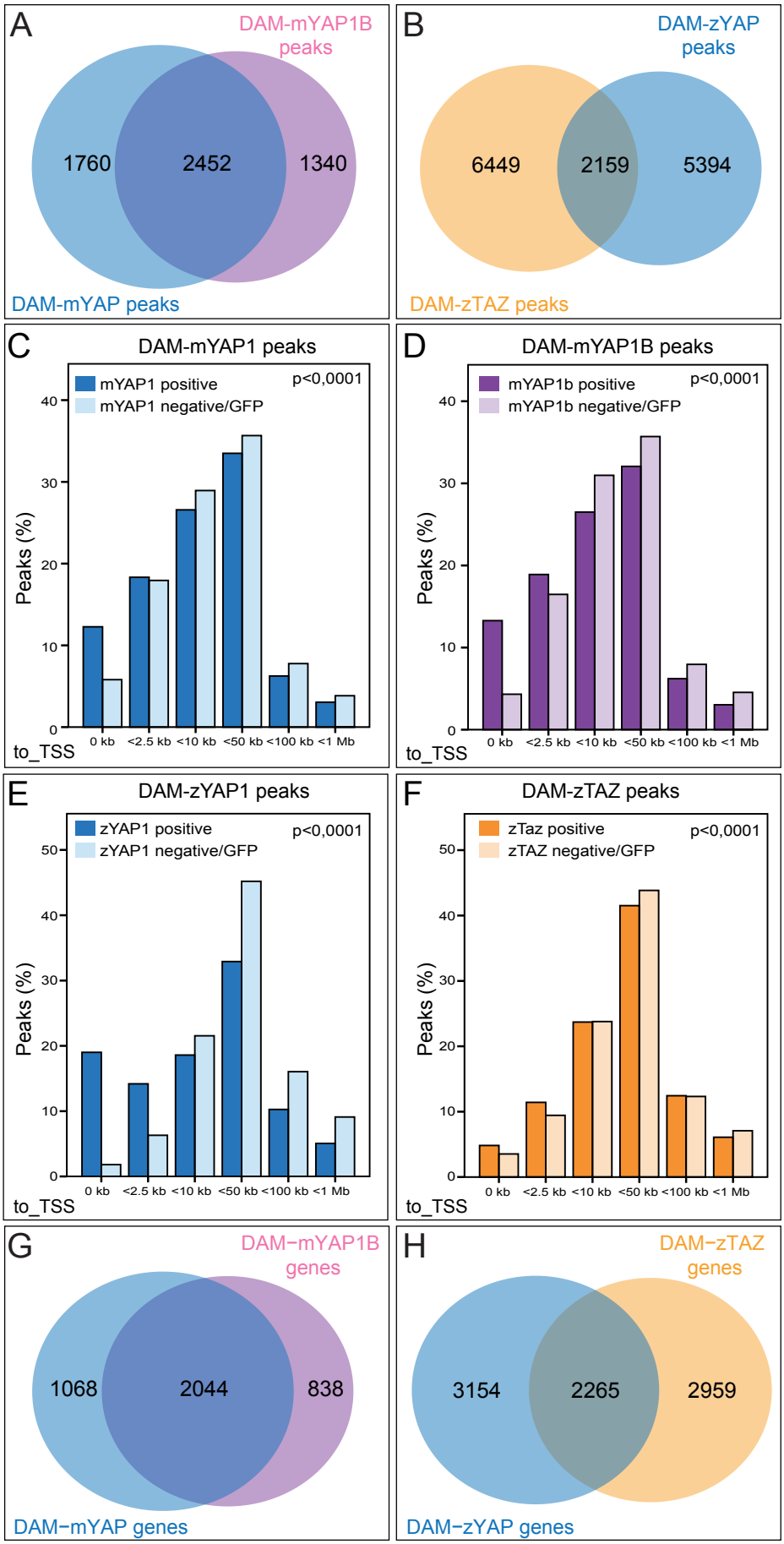

Figure S9: Peaks overlap and distance to the closest TSS. Diagrams show the overlap between medaka Dam-yap1 and Dam-yap1b peaks (A) and zebrafish Dam-yap1 and Dam-taz peaks (B). The distribution of the peaks according to their distance to the neighboring TSS is shown for positive and negative peaks associated to medaka Dam-yap1 (C) and Dam-yap1b (D), and zebrafish Dam-yap1 (E) and Dam-taz (F). Statistical differences in the distribution of positive vs. negative peaks were determined using Chi-square (p values are indicated). The overlap between medaka Dam-yap1 and Dam-yap1b genes (G) and zebrafish Dam-yap1 and Dam-taz genes (H) is also represented.

A

Enriched motifs in zYap1 peaks

Identified motif	Most similar motif	Name	E-value	q-value
		FOX	$1.9 \cdot 10^{-373}$	$5.08 \cdot 10^{-2}$
		TEAD	$7.4 \cdot 10^{-147}$	$2.84 \cdot 10^{-1}$
		SOX	$1.1 \cdot 10^{-145}$	$3.18 \cdot 10^{-2}$
		ZFP161	$7.6 \cdot 10^{-59}$	$1.04 \cdot 10^{-2}$
		ZNF435	$7.4 \cdot 10^{-53}$	$9.67 \cdot 10^{-2}$
		MABF	$9.6 \cdot 10^{-47}$	$2.43 \cdot 10^{-2}$
		YY2	$5 \cdot 10^{-37}$	$2.58 \cdot 10^{-2}$
		TP63	$7.2 \cdot 10^{-30}$	$9.72 \cdot 10^{-2}$
		POU	$3.6 \cdot 10^{-26}$	$7.39 \cdot 10^{-2}$
		HMX2	$5.3 \cdot 10^{-16}$	$3.10 \cdot 10^{-2}$

B

Enriched motifs in zTaz peaks

Identified motif	Most similar motif	Name	E-value	q-value
		EBF1	$3.9 \cdot 10^{-379}$	$9.29 \cdot 10^{-2}$
		RXRA	$1.3 \cdot 10^{-144}$	$1.30 \cdot 10^{-3}$
		TFAP2	$5.5 \cdot 10^{-122}$	$1.57 \cdot 10^{-2}$
		NEUROG2 BHLHE22	$2.7 \cdot 10^{-98}$	$2.45 \cdot 10^{-2}$
		ZNF24	$9.6 \cdot 10^{-66}$	$5.18 \cdot 10^{-3}$
		SMAD3	$1.7 \cdot 10^{-52}$	$8.40 \cdot 10^{-4}$
		ZIC	$3.3 \cdot 10^{-45}$	$7.44 \cdot 10^{-2}$
		HIC1	$7.4 \cdot 10^{-31}$	$3.58 \cdot 10^{-2}$
		EGR1	$3.3 \cdot 10^{-24}$	$8.67 \cdot 10^{-4}$
		TEAD	$9.5 \cdot 10^{-3}$	$2.10 \cdot 10^{-1}$

Figure S10: Analysis of motifs enriched in zebrafish DamID-seq peaks. List of enriched motifs associated to zebrafish Yap1 (A) and Taz (B) peaks, as identified by DREME and recognized by Tomtom. Both DREME E-value and Tomtom q-values are shown. TEAD motif is highlighted with red boxes. TEAD was only the 22nd best-ranked motif in the taz dataset (11 to 21 are not shown).

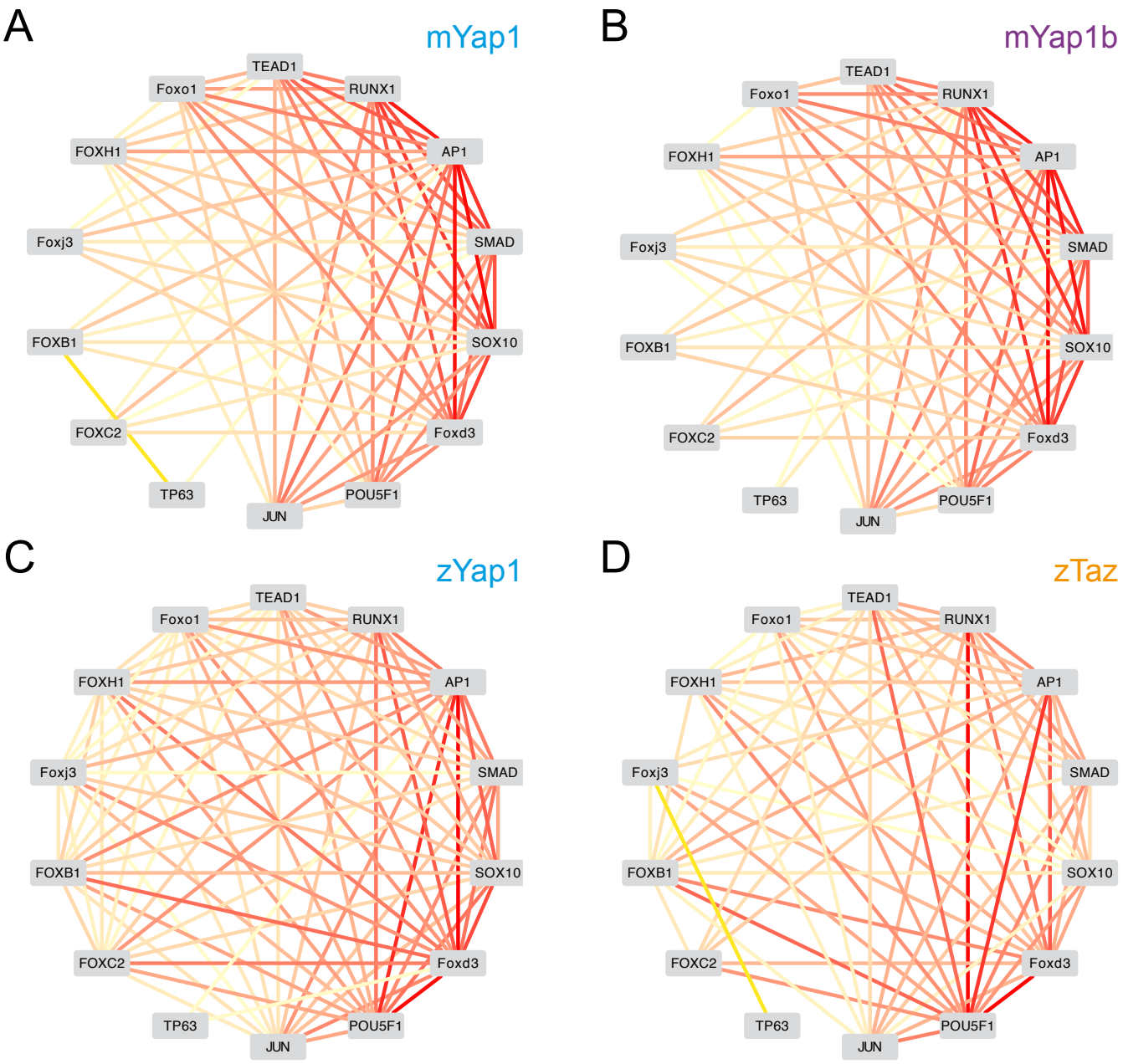

Figure S11: Analysis of co-occurring motifs. Cytoscape network visualization of the significant interaction among identified motifs (see Table S2) within medaka Yap1 (A), medaka Yap1b (B), zebrafish Yap1 (C), and zebrafish Taz (D) DamID peaks. For each edge of the network, the percentage (%) of peaks containing at least one match of both motifs was used to infer the intensity of the interactions between motifs. The color of the edges indicates the strength of these interactions, from 5% (pale yellow) to 16% of the peaks (red).

A

	Chip-seq	Lian et al. 2010		Estaras et al. 2017		Zanconato et al. 2015	
		mESCs	Dif. mESCs	hESCs	hESCs	MDA-MB-231 breast cancer	MDA-MB-231 breast cancer
		Yap1	Yap1	Yap1	Tead4	Yap1	Taz
Dam-ID	#genes	7738	3558	1861	4144	4166	4922
mYap1	3112	1.61E-18	6.14E-09	1.03E-27	3.22E-36	4.76E-23	8.34E-22
mYap1b	2882	4.29E-16	4.12E-12	8.46E-25	6.5E-30	1.01E-22	1.42E-23
zYap1	5419	3.08E-34	7.76E-19	4.47E-32	3.92E-49	9.83E-33	1.19E-33
zTaz	5224	3.51E-30	6.18E-16	2.6E-27	1.11E-50	1.33E-37	3.11E-38
		Significance of overlapping (targeted genes)					

B

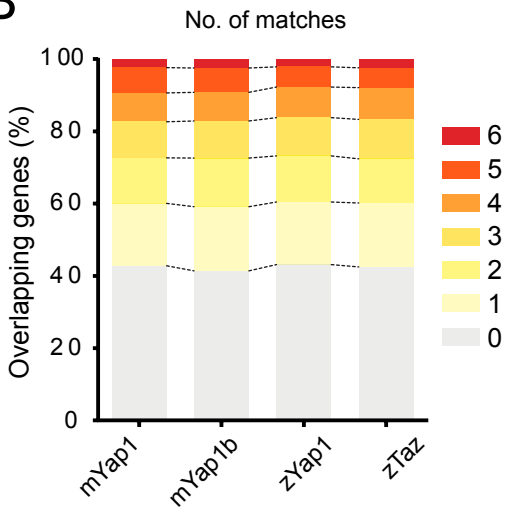

Figure S12: Comparative analysis of targeted genes in Chip-seq and DamID studies. (A) Values included in the table show how significant (hypergeometric test) is the overlap between genes identified as Yap1, Yap1b or Taz targets in our DamID study and identified targeted genes in 6 available Chip-seq datasets. Reference papers, source material and antibodies used are indicated. The number of genes associated either to DamID or Chip-seq peaks is also indicated. Significance levels are highlighted with a color code. (B) The graphics shows the % of medaka Yap1, Yap1b, and zebrafish Yap1 and Taz associated genes overlapping with genes identified in 0 to 6 of the Chip-seq datasets.

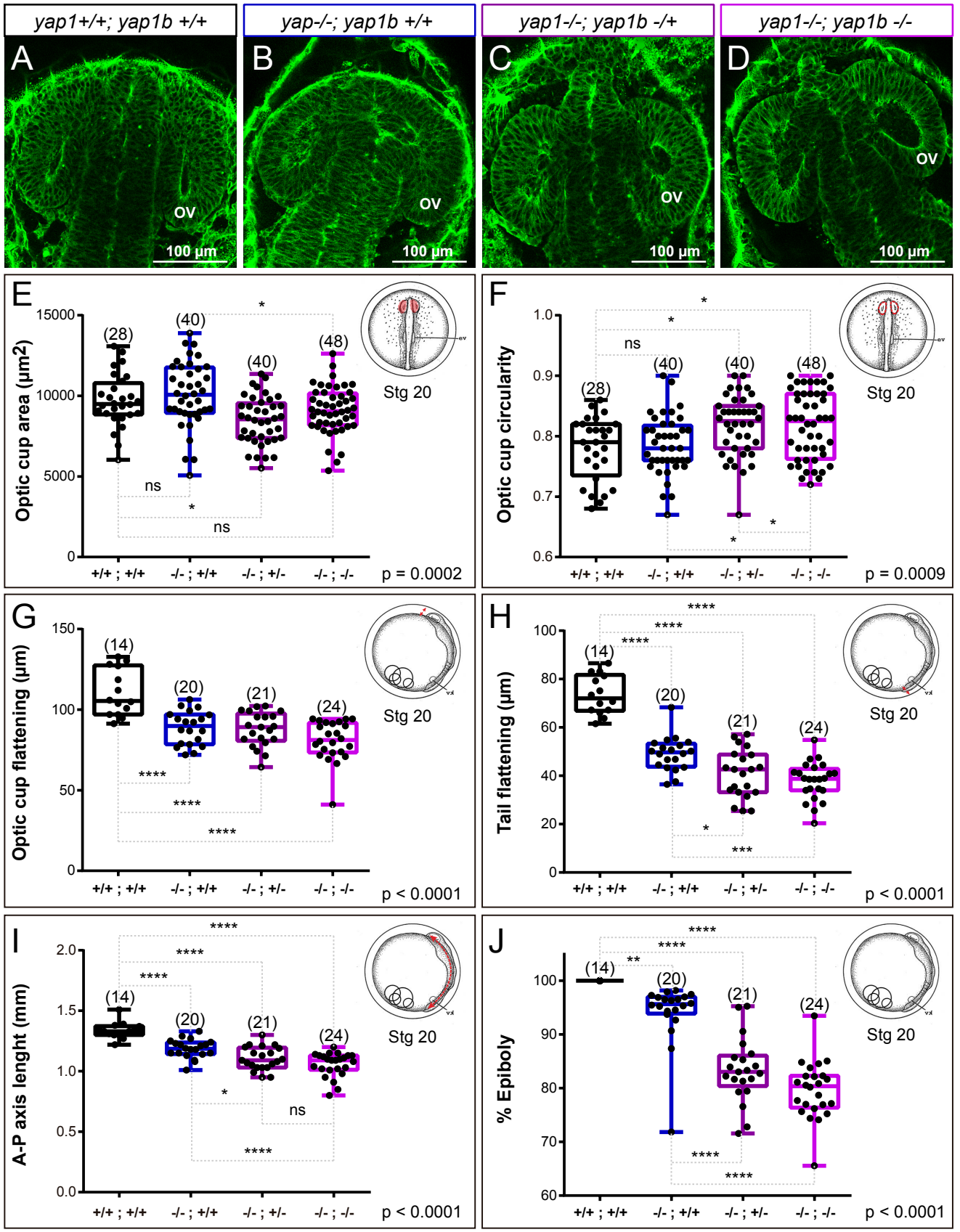

Figure S13: Quantitative analysis of morphogenetic defects in *yap1/yap1b* single and double mutants. (A-D) Confocal sections of phalloidin stained embryos showing optic cup morphology in wild type, *yap1* mutants, and *yap1*/*yap1b* double mutants. (E-J) Quantitative analysis of optic cup area (E), circularity (F), and flattening (G); as well as tail flattening (H), embryo axis lenght (I), and % of epiboly (J) in wild type and mutant embryos reveal enhanced tissue malformations in *yap1/yap1b* double mutants. One Way ANOVA analysis followed by Fisher's LSD test was used to evaluate statistical significance. ov = optic vesicle. Magnification bars are included in the figure.

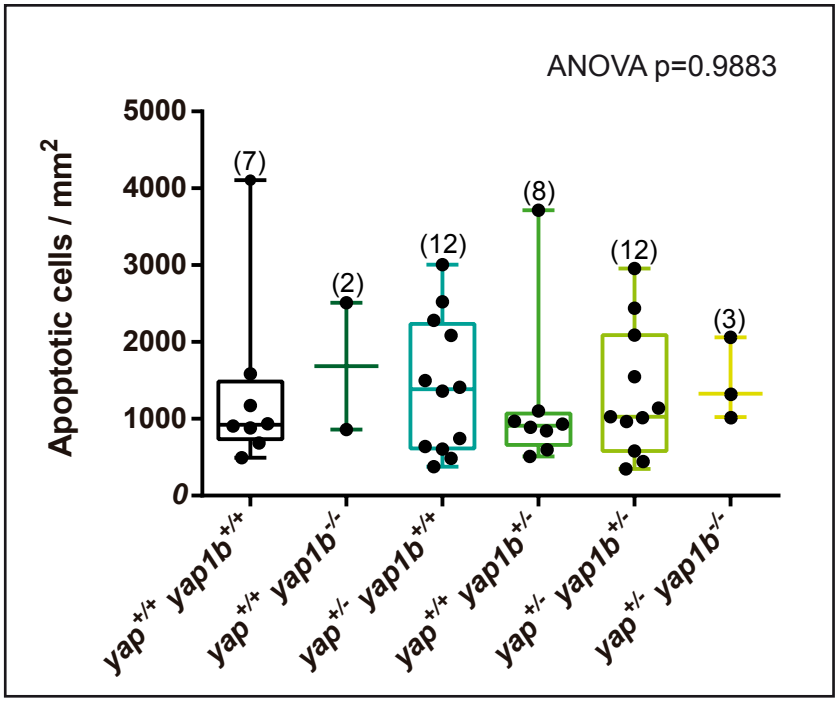

Figure S14: Apoptosis levels in embryos harboring at least one wild type *yap1* allele. Quantification of caspase-3 positive cells per area shows no significant differences as long as a functional copy of *yap1* is present in the genome. One Way ANOVA analysis followed by Fisher's LSD test was used to evaluate statistical significance.

Table S1: (A) List of gene and protein IDs for Yap family members from different species.
(B) Chromosomes/scaffolds and syntenic arrangements are also indicated

A

Species		Gene ID	Protein ID	Genebank protein ID	Chromosome/scaffold
	Yap1	Yap1			
Homo sapiens	Human	ENSG00000137693	ENSP00000478927.1		chr11
Mus musculus	Mouse	ENSMUSG00000053110	ENSMUSP00000069554		chr9
Lepisosteus oculatus	Gar	ENSLOCG00000005660	ENSLOCP00000006836		LG3
Clupea harengus	Herring	XM_012830954.1		XP_012686408.1,	
Danio rerio	Zebrafish	ENSDARG00000068401	ENSDARP00000089684		chr18
Astyanax mexicanus	Mexican tetra	ENSAMXG00000015263	ENSAMXP00000015710.	XP_022520645.1	Scaffold KB871855.1
Oryzias latipes	Medaka	ENSORLG00000002708	ENSORLP00000003377*	XP_004075324.1	ch13
Oreochromis niloticus	Tilapia	ENSONIG00000005729	ENSONIP00000007219.1		GL831218.
Gasterosteus aculeatus	Stickleback	ENSGACG00000012139	ENSGACP00000016062.1		LGI
Gadus morhua	Cod	ENSGMOG00000002826	ENSGMOP00000002984.1		Scaffold_2296
Esox lucius	N. Pike	XM_013135880		XP_012991334	LG1
	Yap1b	Yap1b			
Oryzias latipes	Medaka	ENSORLG00000005573	ENSORLP00000007010*	XP_004076495.1	chr14
Oreochromis niloticus	Tilapia	ENSONIG00000004889	ENSONIP00000006147*	XP_005472252.1	Scaffold GL831183
Gasterosteus aculeatus	Stickleback	ENSGACG00000020627	ENSGACP00000027285		LGVII
Gadus morhua	Cod	ENSGMOG00000002165	ENSGMOP00000002308		Scaffold_4380
Esox lucius	N. Pike	XM_013131740.2		XP_012987194	LG07
	birc2	birc2			
Clupea harengus	Herring	105895386 (birc2)			Scaffold_244
Danio rerio	Zebrafish	ENSDARG00000044619			chr21
Astyanax mexicanus	Mexican tetra	ENSAMXG00000004822			Scaffold_KB882129
	Taz(wwtr1)	Taz(wwtr1)			
Homo sapiens	Human	ENSG00000018408	ENSP00000419465.1		chr3
Mus musculus	Mouse	ENSMUSG00000027803	ENSMUSP00000029380		chr3
Lepisosteus oculatus	Gar	ENSLOCG00000001759	ENSLOCP00000002036		LG14
Clupea harengus	Herring	105898312 (wwtr1)		XP_012680789.1	Scaffold_328
Danio rerio	Zebrafish	ENSDARG00000067719	ENSDARP00000139152		chr22
Astyanax mexicanus	Mexican tetra	ENSAMXG00000004716	ENSAMXP00000004825.1		Scaffold KB871797.1
Esox lucius	N. Pike	XM_020044305.1		XP_019899864.1	Scaffold_0183
Gadus morhua	Cod	na		na	Scaffold_2167
	commd2	commd2			
Oryzias latipes	Medaka	ENSORLG00000002784			chr4
Oreochromis niloticus	Tilapia	ENSONIG00000007638			Scaffold GL831201.1
Gasterosteus aculeatus	Stickleback	ENSGACG00000002117			scaffold_56
Basal Teleost Species		Gene ID	Protein ID	Genebank protein ID	Chromosome/scaffold
	Yap1	Yap1			
Anguilla japonica	Japanese eel	na	na		ANJA007541
Paramormyrops kingsleyae	Elephantfish	na	na		Scaffold84
	Yap1b	Yap1b			
Anguilla japonica	Japanese eel	na	na		ANJA007098
Paramormyrops kingsleyae	Elephantfish	na	na		Scaffold63
	Taz(wwtr1)	Taz(wwtr1)			
Anguilla japonica	Japanese eel	na	na		ANJA001635
Anguilla japonica	Japanese eel	na	na		ANJA000083
Paramormyrops kingsleyae	Elephantfish	na	na		Scaffold797
Paramormyrops kingsleyae	Elephantfish	na	na		Scaffold40

B

	Species	Chromosomal arrangement												
	Yap1													
Homo sapiens	Human	<MamL2	6 Mb	arhgap42>	<trpc6	<angptl5	Cep126>	Yap1>	Birc3>	Birc2>	<tmem123			
Mus musculus	Mouse	<MamL2	5 Mb	arhgap42>	<trpc6		Cep126>	Yap1>	Birc3>	Birc2>	<tmem123			
Lepisosteus oculatus	Gar			arhgap42>	<trpc6	<angptl5	cep126>	Yap1>		Birc2>		<MamL2	<gab2	<nars2
Clupea harengus	Herring						cep126>	Yap1a>				<tbcb		
Danio rerio	Zebrafish			arhgap42b>	<trpc6b	4.5 Mb	cep126>	Yap1>			<tmem123	<tbcb	six5>	
Astyanax mexicanus	Mexican tetra					truncated scaf		Yap1>				<tbcb	six5>	
Oryzias latipes	Medaka			arhgap42b>	<trpc6b			Yap1a>				<MamL2	<gab2	<nars2
Oreochromis niloticus	Tilapia			arhgap42b>	<trpc6b			Yap1a>				<MamL2	<gab2	<nars2
Gasterosteus aculeatus	Stickleback			arhgap42b>	<trpc6b		cep126>	Yap1a>				<MamL2	<gab2	<nars2
Gadus morhua	Cod			arhgap42b>	<trpc6b			Yap1a>				<MamL2	<gab2	<nars2
Esox lucius	N. Pike			arhgap42b>	<trpc6b		cep126>	Yap1a>				<MamL2	<gab2	<nars2
	Yap1b													
Oryzias latipes	Medaka			arhgap42a>	<trpc6a	<angptl5		Yap1b>		Birc2>				
Oreochromis niloticus	Tilapia			arhgap42a>	<trpc6a	<angptl5		Yap1b>		Birc2>				
Gasterosteus aculeatus	Stickleback			arhgap42a>	<trpc6a	<angptl5		Yap1b>		Birc2>				
Gadus morhua	Cod			arhgap42a>	<trpc6a	<angptl5		Yap1b>			truncated scaffold			
Esox lucius	N. Pike				na	na	na	Yap1b>		Birc2>				
	birc2													
Clupea harengus	Herring			arhgap42a>	<trpc6a	<angptl5				Birc2>				
Danio rerio	Zebrafish			arhgap42a>	<trpc6a	<angptl5				Birc2>				
Astyanax mexicanus	Mexican tetra			arhgap42a>	<trpc6a	<angptl5				Birc2>				
	Taz(wwtr1)													
Homo sapiens	Human			hps3>	<tm4sf18	<tm4sf1	tm4sf4>	<taz	<commd2	<ankub1	rnf13>	<pfn2		
Mus musculus	Mouse					<tm4sf1	tm4sf4>	<taz	<commd2	<ankub1	rnf13>	<pfn2		
Lepisosteus oculatus	Gar			hps3>	<tm4sf1	tm4sf4>	tm4sf18>	<taz			rnf13>	<pfn2		
Clupea harengus	Herring			hps3>			tm4sf4>	<taz	<commd2	<ankub1	rnf13>	<pfn2		
Danio rerio	Zebrafish			hps3>	<tm4sf18		tm4sf4>	<taz	<commd2	3 Mb	pfn2>	<rnf132		
Astyanax mexicanus	Mexican tetra			hps3>	<tm4sf18		tm4sf4>	<taz	<commd2	ncated scaffold				
Esox lucius	N. Pike					na	na	<taz	<commd2	na				
Gadus morhua	Cod				truncated scaffold			<taz?	<commd2					
	commd2													
Oryzias latipes	Medaka						ctns>		<commd2					
Oreochromis niloticus	Tilapia						ctns>	<trappc8	<commd2					
Gasterosteus aculeatus	Stickleback						ctns>	<trappc8	<commd2					

	deletion
	insertion
	re-arrangement
	inversion
	truncated scaffolds
na	not annotated

Table S2: List of motifs used to evaluate motifs cooperation

ID	NAME
MA0002.2	RUNX1
MA0030.1	FOXF2
MA0041.1	Foxd3
MA0047.2	Foxa2
MA0077.1	SOX9
MA0078.1	Sox17
MA0090.1	TEAD1
MA0143.3	Sox2
MA0157.2	FOXO3
MA0442.2	SOX10
MA0479.1	FOXH1
MA0480.1	Foxo1
MA0481.2	FOXP1
MA0488.1	JUN
MA0490.1	JUNB
MA0491.1	JUND
MA0513.1	SMAD2::SMAD3::SMAD4
MA0525.2	TP63
MA0593.1	FOXP2
MA0628.1	POU6F1
MA0785.1	POU2F1
MA0786.1	POU3F1
MA0787.1	POU3F2
MA0795.1	SMAD3
MA0845.1	FOXB1
MA0846.1	FOXC2
MA0850.1	FOXP3
MA0851.1	Foxj3
MA0852.2	FOXK1
MA0866.1	SOX21
MA0870.1	Sox1
MA0940.1	AP1
MA1115.1	POU5F1
MA1120.1	SOX13
MA1153.1	Smad4

Table S3: Overrepresented GO-slim terms associated to genes targeted by Yap1 or Yap1b

FDR<0.05; Fold enrichment >1.3
Fisher's Exact test with FDR multiple test correction.

Yap1 medaka

Oryzias latipes (REF) — Client Text Box Input (Hierarchy) NEW!)

PANTHER GO-Slim Molecular Function	#	#	expected	Fold Enrichment	+/-	raw P value	FDR
transmembrane receptor protein tyrosine kinase activity	74	27	11.38	2.37	+	3.19E-04	9.93E-03
sequence-specific DNA binding RNA polymerase II transcription factor activity	258	71	39.69	1.79	+	3.78E-05	2.36E-03
sequence-specific DNA binding transcription factor activity	806	191	124.00	1.54	+	1.42E-07	2.65E-05
binding	4505	785	693.06	1.13	+	2.63E-04	9.83E-03
DNA binding	1027	229	158.00	1.45	+	4.37E-07	4.09E-05

PANTHER GO-Slim Biological Process	#	#	expected	Fold Enrichment	+/-	raw P value	FDR
negative regulation of apoptotic process	119	40	18.31	2.18	+	5.36E-05	3.20E-03
developmental process	1479	316	227.53	1.39	+	8.11E-08	1.94E-05
ectoderm development	230	69	35.38	1.95	+	4.37E-06	5.22E-04
embryo development	104	31	16.00	1.94	+	2.08E-03	4.97E-02
cell differentiation	488	117	75.08	1.56	+	2.69E-05	2.14E-03
anion transport	272	65	41.85	1.55	+	2.06E-03	5.47E-02
regulation of phosphate metabolic process	535	115	82.31	1.40	+	1.53E-03	5.21E-02

PANTHER Protein Class	#	#	expected	Fold Enrichment	+/-	raw P value	FDR
transcription factor	1088	253	167.38	1.51	+	4.58E-09	9.85E-07

Yap1b medaka

Oryzias latipes (REF) — Client Text Box Input (Hierarchy NEW!)

PANTHER GO-Slim Molecular Function	#	#	expected	Fold Enrichment	+/-	raw P value	FDR
transmembrane receptor protein tyrosine kinase activity	74	30	10.55	2.84	+	7.54E-06	1.41E-03
sequence-specific DNA binding RNA polymerase II transcription factor activity	258	63	36.78	1.71	+	2.33E-04	1.09E-02
sequence-specific DNA binding transcription factor activity	806	166	114.90	1.44	+	2.33E-05	2.17E-03

PANTHER GO-Slim Biological Process	#	#	expected	Fold Enrichment	+/-	raw P value	FDR
negative regulation of apoptotic process	119	39	16.96	2.30	+	2.72E-05	1.63E-03
developmental process	1479	314	210.83	1.49	+	1.27E-10	3.04E-08
embryo development	104	32	14.83	2.16	+	3.52E-04	1.05E-02
ectoderm development	230	65	32.79	1.98	+	4.62E-06	3.68E-04
transmembrane receptor protein tyrosine kinase signaling pathway	157	43	22.38	1.92	+	3.34E-04	1.14E-02
MAPK cascade	314	75	44.76	1.68	+	1.35E-04	6.43E-03
cell differentiation	488	114	69.57	1.64	+	4.46E-06	5.33E-04
cell adhesion	334	72	47.61	1.51	+	1.85E-03	4.91E-02
biological adhesion	334	72	47.61	1.51	+	1.85E-03	4.42E-02
regulation of phosphate metabolic process	535	112	76.27	1.47	+	2.83E-04	1.13E-02

PANTHER Protein Class	#	#	expected	Fold Enrichment	+/-	raw P value	FDR
transcription factor	1088	222	155.10	1.43	+	1.31E-06	2.81E-04

Common Yap1 & Yap1b

Oryzias latipes (REF) — Client Text Box Input (Hierarchy NEW!)

PANTHER GO-Slim Molecular Function	#	#	expected	Fold Enrichment	+/-	raw P value	FDR
sequence-specific DNA binding transcription factor activity	806	154	113.34	1.36	+	5.26E-04	4.92E-02
DNA binding	1027	196	144.42	1.36	+	9.64E-05	1.80E-02

PANTHER GO-Slim Biological Process	#	#	expected	Fold Enrichment	+/-	raw P value	FDR
negative regulation of apoptotic process	119	32	12.05	2.66	+	6.35E-06	7.59E-04
developmental process	1479	226	149.76	1.51	+	9.28E-09	2.22E-06
transmembrane receptor protein serine/threonine kinase signaling pathway	69	18	6.99	2.58	+	1.05E-03	2.79E-02
embryo development	104	24	10.53	2.28	+	6.34E-04	2.16E-02
ectoderm development	230	47	23.29	2.02	+	3.64E-05	2.17E-03
transmembrane receptor protein tyrosine kinase signaling pathway	157	31	15.90	1.95	+	1.34E-03	3.21E-02
regulation of cell cycle	170	32	17.21	1.86	+	2.09E-03	4.55E-02
MAPK cascade	314	56	31.79	1.76	+	1.84E-04	7.34E-03
cell differentiation	488	86	49.41	1.74	+	6.73E-06	5.36E-04
regulation of phosphate metabolic process	535	86	54.17	1.59	+	1.30E-04	6.23E-03

PANTHER Protein Class	#	#	expected	Fold Enrichment	+/-	raw P value	FDR
transcription factor	1088	167	110.17	1.52	+	7.52E-07	1.62E-04

Table S4: List of primers used in this work. Their name, sequence, and application are indicated.

Nº	Name	Sequence (5' - 3')	Application
1	mYapKOsg#3_TAGG	TAGGCACGTCGTCGGGAATCTCGT	*Generation of yap1 mutants (sgRNA)*
2	mYapKOsg#3_AAAC	AAACACGAGATTCCCGACGACGTG	*Generation of yap1 mutants (sgRNA)*
3	mYapKOsg#4_TAGG	TAGGATCTCGTAGGACGACTGC	*Generation of yap1 mutants (sgRNA)*
4	mYapKOsg#4_AAAC	AAACGCAGTCGTCCTACGAGAT	*Generation of yap1 mutants (sgRNA)*
5	mYapKOsg#5_TAGG	TAGGGACGAGTGTGCGCGTACG	*Generation of yap1 mutants (sgRNA)*
6	mYapKOsg#5_AAAC	AAACCGTACGCGCACACTCGTC	*Generation of yap1 mutants (sgRNA)*
7	Crispr mYAP Fw	CAGCCCACAAAACATACAGTTTA	*Genotyping of yap1 mutants*
8	Crispr mYAP Rv	AAGATCTGCTGGGAGAACTCTTT	*Genotyping of yap1 mutants*
9	sgRNA mYAP1B #1	taatacgactcactataGGGGGGAGTGGCACATCGTCgttttagagctagaa	*Generation of yap1b mutants (sgRNA)*
10	sgRNA mYAP1B #2	taatacgactcactataGGCGGGGAGCGCAGCGGGGGgttttagagctagaa	*Generation of yap1b mutants (sgRNA)*
11	CRISPR mYAP1B Fw	TTTAAAGAAACCTGCAGAGCAAC	*Genotyping of yap1b mutants*
12	CRISPR mYAP1B Rv	AGCAACATGTCCAATTAAAAACC	*Genotyping of yap1b mutants*
13	OL-YAP Fw-SpeI	AATTTactagtATGGATCCGAGCCAGCACAACCCTC	Generation of Dam-TF fusions
14	OL-YAP Rv-XbaI	AATTTtctagaTTATAACCATGTGAGGAAGCTCTC	Generation of Dam-TF fusions
15	OL-YAP1B Fw-SpeI	AATTTactagtATGGACGCGCACCGGAGCGGACG	Generation of Dam-TF fusions
16	OL-YAP1B Rv-NheI	AATTTgctagcCTATAGCCAGGTGAGCAGATTGTC	Generation of Dam-TF fusions
17	DR-YAP Fw-SpeI	AATTTactagtATGGATCCGAACCAGCACAAC	Generation of Dam-TF fusions
18	DR-YAP Rv-NheI	AATTTgctagcCTATAGCCAGGTTAGAAAGTTC	Generation of Dam-TF fusions
19	DR-TAZ Fw-SpeI	AATTTactagtATGAGCGGTAATCCTCTCCAGC	Generation of Dam-TF fusions
20	DR-TAZ Rv-XbaI	AATTTtctagaTTAGAGCCAGGTGAGGAAGGGCTC	Generation of Dam-TF fusions
21	AdRt	CTAATACGACTCACTATAGGGCAGCGTGGTCGCGGCCGAGGA	Adaptor primers for DamID
22	AdRb	TCCTCGGCCG	Adaptor primers for DamID
23	AdR_PCRprimer	G*G*T*C*G*C*GGCCGAGGATC	phosphorothioate primer for DamID
24	ISH yap MDK Fw	ACTCCAGATGACTTCCTCAACAG	Generation of templates for ISH
25	ISH yap MDK Rv	AGCCTTGAAGACACAGACACAAT	Generation of templates for ISH
26	ISH yap1b MDK Fw	CCCTGTTCAGTAGGGTGATGA	Generation of templates for ISH
27	ISH yap1b MDK Rv	TACATCTCTCCCTCTGGAGTCAC	Generation of templates for ISH
28	qPCR zEF1A Fw	TCCACCGGTCACCTGATCTACA	Primers for qPCR y ddPCR
29	qPCR zEF1A Rv	CAACACCCAGGCGTACTTGA	Primers for qPCR y ddPCR
30	qPCR zYAP Fw	ATGAACCCAGCCTCAGGTCC	Primers for qPCR y ddPCR
31	qPCR zYAP Rv	TCCAGCCAAGAGGTGGTTTT	Primers for qPCR y ddPCR
32	qPCR zTAZ Fw	TTCCTCAACAGTGGGCCGTA	Primers for qPCR y ddPCR
33	qPCR zTAZ Rv	AGTGGTCGGGATGCTGTAAC	Primers for qPCR y ddPCR
34	qPCR mEF1A Fw	AAACCCAGAAACACCGAAACAT	Primers for qPCR y ddPCR
35	qPCR mEF1A Rv	CCTCCGCACTTGTAGATCAG	Primers for qPCR y ddPCR
36	qPCR mYAP Fw	GTTGAACCAGGCTACCCCTC	Primers for qPCR y ddPCR
37	qPCR mYAP Rv	AGGTCCACTAGCTGGGCTTA	Primers for qPCR y ddPCR
38	qPCR mYAP1B Fw	GTCAACCCGGAGTCAGGTCC	Primers for qPCR y ddPCR
39	qPCR mYAP1B Rv	AGTACATCTCTCCCTCTGGAGTC	Primers for qPCR y ddPCR
40	cyr61 Fw	GAGCTCTCCCTGCCCAATTT	Primers for qPCR
41	cyr61 Rv	CTGTATGCAGGCAGGGTCTT	Primers for qPCR
42	marcksl1b Fw	AAGACCAACGGACAGGAGAAC	Primers for qPCR
43	marcksl1b Rv	CTTCGGGTTTGGTGGCTTCC	Primers for qPCR
44	amotl2a Fw	GCGGCGCAAAGAGATACAAC	Primers for qPCR
45	amotl2a Rv	TGTGGATGGTAGGGACGGAT	Primers for qPCR
46	lats2 Fw	AACGAGCAACTTTTTCCCGC	Primers for qPCR
47	lats2 Rv	CATCTGCGCCATGTGTGATG	Primers for qPCR
48	ctgfa Fw	GCCGACAGGAGATCCACTTG	Primers for qPCR
49	ctgfa Rv	CCTGCAGCCGCGTATGAGTA	Primers for qPCR
50	boka Fw	ACATCTTCTCCACTGGTATCACG	Primers for qPCR
51	boka Rv	TCAACCACACGGTCAGACTC	Primers for qPCR
52	yap1 Fw	GTTGAACCAGGCTACCCCTC	Primers for qPCR
53	yap1 Rv	AGGTCCACTAGCTGGGCTTA	Primers for qPCR
54	yap1b Fw	GTCAACCCGGAGTCAGGTCC	Primers for qPCR
55	yap1b Rv	AGTACATCTCTCCCTCTGGAGTC	Primers for qPCR
56	ef1a Fw	AAACCCAGAAACACCGAAACAT	Primers for qPCR
57	ef1a Rv	CCTCCGCACTTGTAGATCAG	Primers for qPCR

Table S5: List of genomic coordinates for peaks associated to Yap family members

Click here to download Table S5

Table S6: List of genes identified by DamID as Yap1, Yap1b or Taz targets identified also in previous ChIP-seq analyses

Click here to download Table S6